AWARD NUMBER: W81XWH-12-1-0356

TITLE: A Specific Screening Strategy to Reduce Prostate Cancer Mortality

PRINCIPAL INVESTIGATOR: Kurt R. Zinn

CONTRACTING ORGANIZATION: University of Alabama at Birmingham
Birmingham, AL 35294

REPORT DATE: September 2014

TYPE OF REPORT: Annual

PREPARED FOR: U.S. Army Medical Research and Materiel Command
Fort Detrick, Maryland 21702-5012

DISTRIBUTION STATEMENT: Approved for Public Release;
Distribution Unlimited

The views, opinions and/or findings contained in this report are those of the author(s) and should not be construed as an official Department of the Army position, policy or decision unless so designated by other documentation.

REPORT DOCUMENTATION PAGE

1. REPORT DATE	2. REPORT TYPE	3. DATES COVERED
September 2014	Annual	15 Aug 2013 -14 Aug 2014

4. TITLE AND SUBTITLE

A Specific Screening Strategy to Reduce Prostate Cancer Mortality

5a. CONTRACT NUMBER

5b. GRANT NUMBER
W81XWH-12-1-0356

5c. PROGRAM ELEMENT NUMBER

6. AUTHOR(S)

Kurt R. Zinn

E-Mail: kurtzinn@uab.edu

5d. PROJECT NUMBER

5e. TASK NUMBER

5f. WORK UNIT NUMBER

7. PERFORMING ORGANIZATION NAME(S) AND ADDRESS(ES)

University of Alabama at Birmingham
Birmingham, AL 35294

8. PERFORMING ORGANIZATION REPORT NUMBER

9. SPONSORING / MONITORING AGENCY NAME(S) AND ADDRESS(ES)

U.S. Army Medical Research and Materiel Command
Fort Detrick, Maryland 21702-5012

10. SPONSOR/MONITOR'S ACRONYM(S)

11. SPONSOR/MONITOR'S REPORT NUMBER(S)

12. DISTRIBUTION / AVAILABILITY STATEMENT

Approved for Public Release; Distribution Unlimited

13. SUPPLEMENTARY NOTES

14. ABSTRACT

Here, we report the use of a cancer-specific promoter, inhibition of differentiation-1 (Id1), to drive a dual-reporter system (Ad5/3-Id1-SEAP-Id1-mCherry) designed for detection of prostate cancer using a blood-based reporter-secreted embryonic alkaline phosphatase (SEAP) and tumor visualization using a fluorescent reporter protein, mCherry. In human prostate tumors, Id1 levels are correlated with increased Gleason grade and disease progression. To evaluate in vivo performance, flank tumors were grown in athymic male mice using three prostate cancer cell lines. Following intra-tumoral injection of the vector, tumors formed by cells with high Id1 had the greatest reporter expression. Interestingly, tumors with the lowest levels of Id1 and reporter expression produced the greatest amounts of PSA. These data support the use of Ad5/3-Id1-SEAP-Id1-mCherry as a predictor of prostate cancer malignancy and as a strategy for tumor localization. This strategy would assist clinicians in the detection and treatment of prostate cancer and ultimately reduce the mortality associated with this disease.

15. SUBJECT TERMS
prostate cancer screening, imaging, ID1

16. SECURITY CLASSIFICATION OF:			17. LIMITATION OF ABSTRACT	18. NUMBER OF PAGES	19a. NAME OF RESPONSIBLE PERSON USAMRMC
a. REPORT	**b. ABSTRACT**	**c. THIS PAGE**	Unclassified	45	19b. TELEPHONE NUMBER (include area code)
Unclassified	Unclassified	Unclassified			

Table of Contents

1. Introduction:

The goal of the proposed research is early detection of relevant prostate cancer to reduce mortality of the disease. This will be accomplished by introduction of an improved and more specific diagnostic procedure. According to the American Cancer Society, prostate cancer is the second leading cause of cancer-related deaths in men. It is estimated that 1 man in every 36 will die of prostate cancer during their lifetime. This accounts for 33,720 men in 2011. Early and accurate detection of prostate cancer is an urgent priority. Our research strategy will introduce a new paradigm in prostate cancer detection, moving beyond prostate-specific antigen (PSA) screening into an advanced and specific strategy to improve detection and resection, and thereby reduce prostate cancer mortality.**We hypothesize that an effective strategy for the detection of prostate cancer will use Id1 to direct a combined blood-based monitoring and imaging system following systemic delivery and controlled release in the prostate vasculature.** This diagnostic system includes a secreted human embryonic alkaline phosphatase reporter for blood-based monitoring and a mCherry reporter for localized imaging, both under the control of an Id1 promoter, and packaged in an Adenovirus for ease in testing. Id1 expression has been shown to be specific for malignant cancers and will permit differentiation between aggressive cancer and benign hyperplasia. To permit non-invasive and effective systemic delivery of the diagnostic Ad, US contrast agents, or MBs, will be used to deliver the diagnostic vector to the tumor in an US-targeted strategy.

2. Keywords: prostate cancer screening, Imaging, Id1

3. Overall Project Summary:

The accomplishments associated with the three specific aims are summarized below. All of the accomplishments have been included in manuscripts, either published or approaching submission. The manuscripts are included as appendices and provide all details of the methods used.

Task 1. **Specific Aim #1: Correlate prostate cancer phenotype with SEAP/mCherry levels achieved with the diagnostic vector (Ad5/3-Id1-SEAP-Id1-mCherry), an existing vector encoding SEAP and mCherry.** *(Primarily first year, except aim1d that may run in to 2nd year)*

a. **Ad3 receptor expression characterization: A prostate cancer cell panel (PC3, LNCaP, CA-HPV-10, RWPE-1, VCAP, MDA PCA 2b, WPMY-1, DU145) will be analyzed for Ad3 receptor expression.** *(Months 1-4)*

Accomplishment: Ad3 receptor surface expression was quantified for each cell type in the panel by infection with an Ad5/3-CMV-Luc adenovirus. Luciferase counts were subsequently used to normalize diagnostic reporter expression, accounting for differences in Ad5/3-Id1-SEAP-Id1-mCherry infectivity among the cells. SEAP and mCherry reporter expressions were therefore only a reflection of Id1 promoter activity. Results are reported under task 1c, together with results for ID1 expression.

b. The panel of cell lines will be characterized for Id1 promoter expression. *(Months 1-6)*

Accomplishment: Id1 expression, but not PSA level, is an indicator of prostate cancer cell aggressiveness. Six prostate cell lines purchased from ATCC were categorized based on their reported behaviors and measured levels of PSA secretion (Table 1). Normal prostate cells (WPMY-1) secreted a baseline amount of 314.1±8.1 pg/mL PSA. Two of the four cell lines with reportedly aggressive phenotypes (Du145 and PC3) had relatively lower PSA levels, ranging from 230-266 pg/mL, whereas the remaining aggressive cells lines (VCaP and MDA-PCA-2b) had significantly greater levels of PSA as compared to baseline. The one non-aggressive cell type, LNCaP, also secreted significantly increased amounts of PSA in comparison to baseline levels. Id1 expression was elevated in all prostate cancer cell types with reportedly aggressive behaviors compared to normal prostate cells and cancerous cells with a less invasive and non-aggressive phenotype (Figure 1a). No correlation was found between Id1 expression and PSA level (R^2=0.058; Figure 1b).

Table 1. Description of cell lines used for analyses of Ad5/3-Id1-SEAP-Id1-mCherry diagnostic efficacy.

Cell Line	Origin	Behavior	PSA (pg/mL)
WPMY-1	Normal stromal myofibroblast	Normal	324.6±21.5
Du145	Brain metastasis	Aggressive	230.1±8.3[**]
PC3	Bone metastasis	Aggressive	266.2±36.7[*]
VCaP	Vertebral metastasis	Aggressive	762.9±36.4[**]
MDA-PCA-2b	Bone metastasis	Aggressive	11,227±1274[**]
LNCaP	Node metastasis	Non-Aggressive	13,042±315[**]

PSA values reported as mean±SEM (n=3). *p<0.05 and **p<0.001 versus WPMY-1 level.
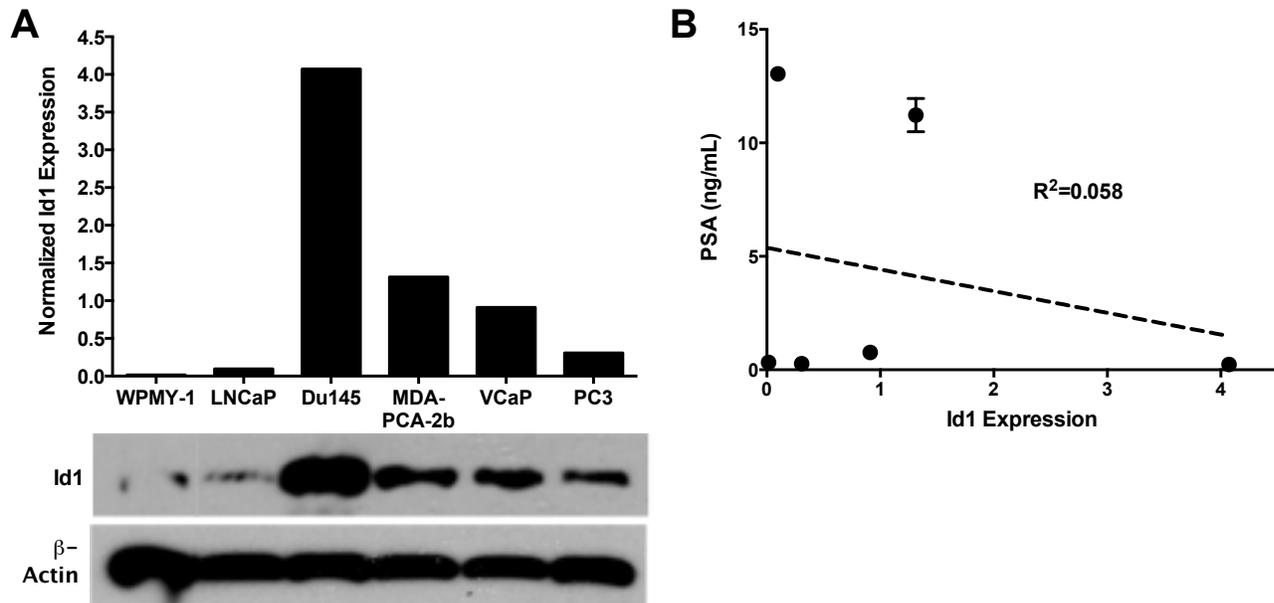
Figure 1. Cellular expression of Id1 does not correlate with PSA. (a) Id1 expression was evaluated in cell lysates by Western blot and quantified with densitometry. Id1 intensity was normalized to the corresponding level of of β-actin. **(b)** Linear regression analysis was used to correlate cellular Id1 expression with PSA levels reported in Table 1. PSA data are shown as mean±SEM (n=3).

c. **Diagnostic vector infection of prostate cancer panel: The performance of the diagnostic vector with the cell panel will be evaluated. Reporter values will be normalized against Ad3 receptor expression. Id1 knockdown experiments will be conducted.** *(Months 6-12)*

Accomplishment: SEAP and mCherry reporter expression correlate with Id1 levels and are indicators of prostate cell aggressiveness As stated under 1a, Ad3 receptor surface expression was quantified for each cell type in the panel by infection with an Ad5/3-CMV-Luc adenovirus (Figure 2a). Luciferase counts were subsequently used to normalize diagnostic reporter expression, accounting for differences in Ad5/3-Id1-SEAP-Id1-mCherry infectivity among the cells. SEAP and mCherry reporter expressions were therefore only a reflection of Id1 promoter activity. After infection with Ad5/3-Id1-SEAP-Id1-mCherry, the prostate cancer lines with aggressive phenotypes (VCaP, MDA-PCA-2b, PC3, and Du145) had increased levels of SEAP reporter compared to non-aggressive (LNCaP) and normal (WPMY-1) cells (Figure 2b). For PC3 and Du145, Ad3-normalized SEAP expression was significantly elevated at 4 and 6 days post-infection compared to non-aggressive LNCaP cells at the corresponding timepoints. A significant correlation (R^2=0.89) between SEAP reporter expression at day 4 and cellular Id1 levels was observed (Figure 2c). Likewise, representative fluorescent images of the mCherry reporter qualitatively confirmed diagnostic vector efficiency (Figure 3). mCherry intensity corresponded to cellular Id1 levels, with the greatest fluorescence observed in the aggressive Du145 cells.

Figure 2. SEAP reporter expression in the prostate cell panel and its relationship with cellular Id1. (a) Susceptibility for infection via the Ad3 fiber serotype was determined for each cell type using Ad5/3-CMV-Luc (multiplicity of infection =1). Luciferase activity was used to normalize diagnostic reporter expression for differences in vector infectivity due to varying levels of Ad3 receptor expression. (b) SEAP reporter was measured in culture medium 2, 4 and 6 days post infection with Ad5/3-Id1-SEAP-Id1-mCherry (multiplicity of infection=1) and normalized with luciferase activity. *P<0.01 vs LNCap at corresponding time point. All data are reported as mean ±s.e.m. (n=4). (c) Cells types were group based on low (o0.25 a.u.), moderate (0.25–1.5 a.u.) or high (41.5 a.u.) Id1 levels and SEAP reporter expression averaged for each group. The low-Id1 group consisted of two cell types (WPMY-1 and LNCaP), the moderate-Id1 group consisted of three cells types (PC3, VCaP

and MDA-PCA-2b) and the high-Id1 group consisted of one cell type (Du145). *P<0.01vs low and **P<0.001 vs all groups.
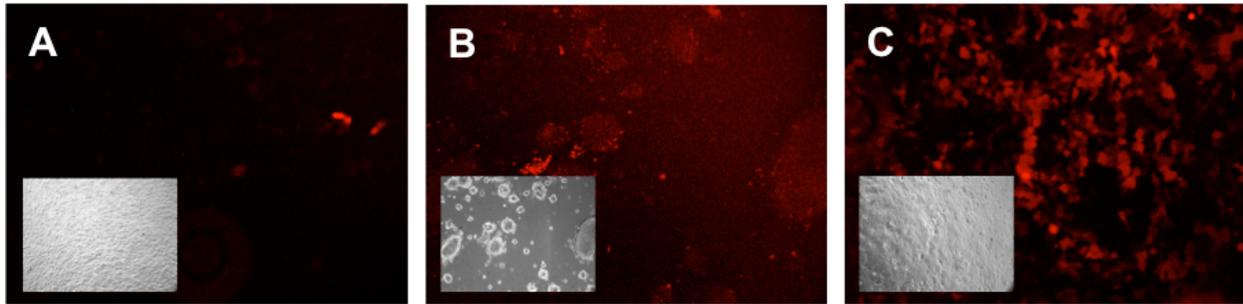
Figure 3. mCherry reporter fluorescence corresponds to prostate cancer cell aggressiveness. Representative fluorescence images of **(a)** normal prostate cells (WPMY-1) and cancerous cells with **(b)** moderate Id1 expression (VCaP) and **(c)** high Id1 expression (Du145). Inserts are corresponding bright field images. All images were acquired using a 10X objective.

d. **Assessment of the diagnostic potential of the vector on normal, BPH, and malignant tissue samples of the prostate: In addition to reporter expression characterization, Id1 and Ad3 expression will be evaluated and normalized against reporter values. (n=10/group)***(Months 1-18)*

Accomplishment. A mechanism was established to obtain fresh prostate tissues following surgery, with support from UAB surgeon Dr. Sudarshan (Co-Investigator of this DOD grant) and pathologist Dr. Shi Wei. Studies were conducted with two surgical specimens that were subdivided into replicates that allowed us to establish conditions for infection with the diagnostic Ad (Ad5/3-Id1-SEAP-Id1-mCherry). Representative images are shown below in Figure 4, and show clusters of mCherry-positive cells. These images were collected with a spectral camera, so the fluorescence is specific for the fluorescence emission of mCherry. The profile for mCherry emission was not found in any control samples that were not infected with the Ad vector. The positive areas in Figure 4b-d are presumed to be clusters of aggressive cancer, but we await confirmation by Dr. Wei, our collaborator for these studies. Adjacent tissues were saved for histology analyses. We are also in the process of conducting the SEAP analyses of the media collected over time. During year 3 we will complete the additional studies with the patient samples.
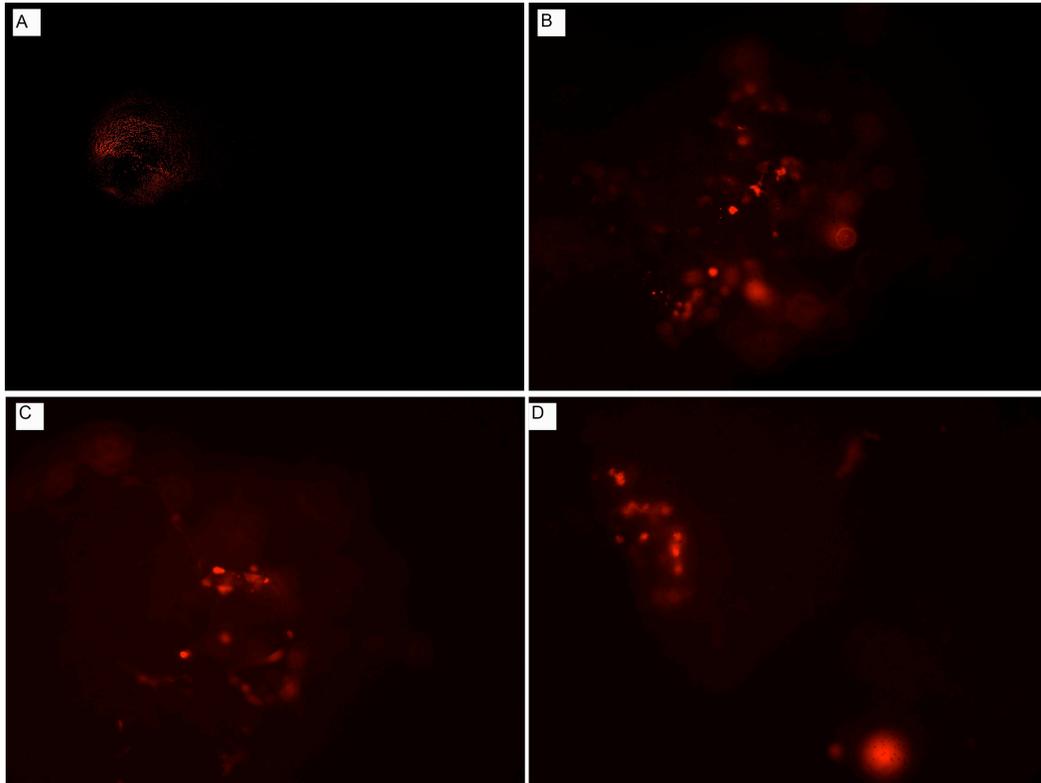
Figure 4. Representative fluorescent images of mCherry expression at 5 days following infection of fresh human prostate surgery tissues with (a) no Ad (control) and (b-d) Ad5/3-Id1-SEAP-Id1-mCherry.

Task 2. Specific Aim #2: Optimize and validate Ad5/3-Id1-SEAP-Id1-mCherry loading of ultrasound microbubbles. *(Start month 9, ending at month 18 (middle of year 2))*

a. Qualitative visualization of Ad packaged microbubbles: Using fluorescent confocal microscopy, microbubble packaged, fluorescent Ad particles containment will be analyzed. *(Months 9-12)*

Accomplishment.   We decided that before packaging experiments it was important to understand if the ultrasonograpy would change Ad infectivity due to disruption of the Ad particles. We also sought to understand if microbubbles with ultrasound would aid in allowing the Ad particle to better infect prostate cancer cells. The results of these studies are summarized below in the abstract of a published manuscript entitled "Enhancement of Adenovirus Delivery after Ultrasound-Stimulated Therapy in a Cancer Model".

Improving the efficiency of adenovirus (Ad) delivery to target tissues has the potential to advance the translation of cancer gene therapy. Ultrasound (US)-stimulated therapy utilizes

microbubbles (MBs) exposed to low-intensity US energy to improve localized delivery. We hypothesize that US-stimulated gene therapy can improve Ad infection in a primary prostate tumor through enhanced tumor uptake and retention of the Ad vector. *In vitro* studies were performed to analyze the degree of Ad infectivity after application of US-stimulated gene therapy. A luciferase-based Ad on a ubiquitous cytomegalovirus (CMV) promoter (Ad5/3-CMV-Luc) was used in an animal model of prostate cancer (bilateral tumor growth) to evaluate Ad transduction efficiency after US-stimulated therapy. Bioluminescence imaging was employed for *in vivo* analysis to quantify Ad infection within the tumor. *In vitro* studies revealed no difference in Ad transduction between groups receiving US-stimulated therapy using high, low, or sham US intensity exposures at various multiplicity of infections (MOIs) ($p = 0.80$). *In vivo* results showed that tumors receiving US-stimulated therapy after intratumoral injection of Ad5/3-CMV-Luc (1×10^6 plaque forming units) demonstrated a 95.1% enhancement in tumor delivery compared to control tumors receiving sham US ($p = 0.03$). US-stimulated therapy has significant potential to immediately impact Ad-based cancer gene therapy by improving virus bioavailability in target tissues.

Accomplishment.   In year 2 we evaluated encapsulation of fluorescent Ad vector by confocal imaging. A representative image is show in Figure 5.
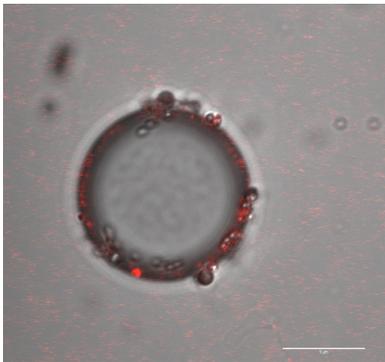
Figure 5. Representative image of microbubble with encapsulated fluorescent Ad particles.

b. Evaluation of human complement to effectively inactivate unencapsulated and partial encapsulated particles: Surrogate Ad particle inactivation with human complement will be evaluated. (Months 12-14)

Accomplishment. In vitro assays were performed to determine the effect of complement on Ad particle infectivity. These data were utilized for subsequent experiments to sufficiently inactivate unenapsulated and partially encapsulated particles following microbubble packaging.
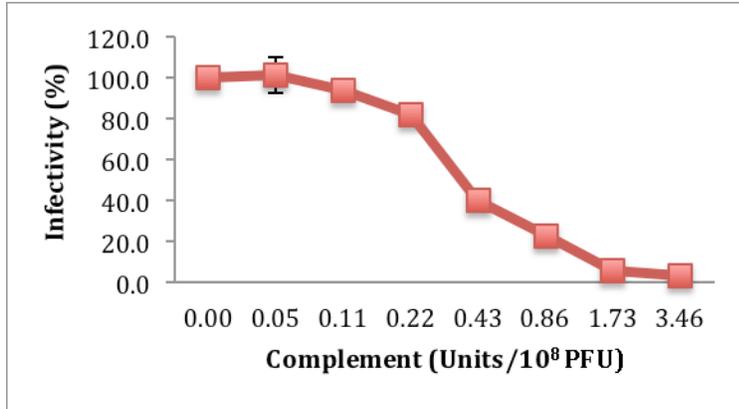
Figure 6. Effect of complement on Ad infectivity.

c. Quantification of functional Ad packaged per microbubble: The number of functional Ad particles successfully packaged within the microbubbles will be determined. *(Months 15-17)*

Accomplishment. Using fluorescently-labeled Ad particles and flow cytometry, we determined that approximately 6% of microbubbles contain Ad particles following the encapsulation process (Figure 7). The functionality of these Ad-packaged microbubbles was determined by measuring the level of cellular infectivity with and without complement inactivation (Figure 8).
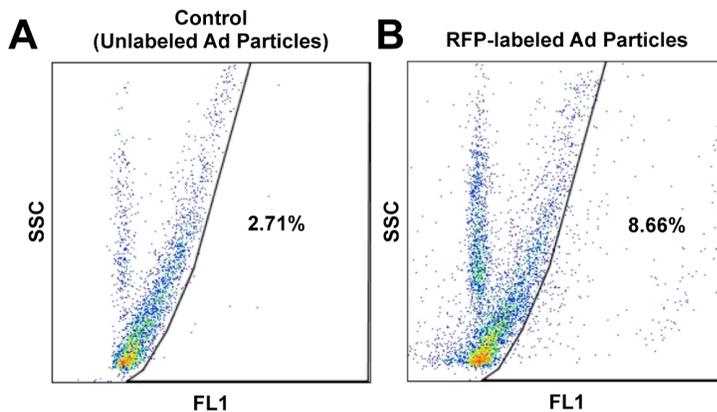
Figure 7. Quantification of microbubbles containing Ad particles. The percentage of microbubbles packaged with Ad particles was determined using (A) unlabeled Ad particles and (B) Ad particles labeled with red fluorescent protein (RFP). The population with increased fluorescence (FL1) was identified as the microbubbles packaged with Ad particles.
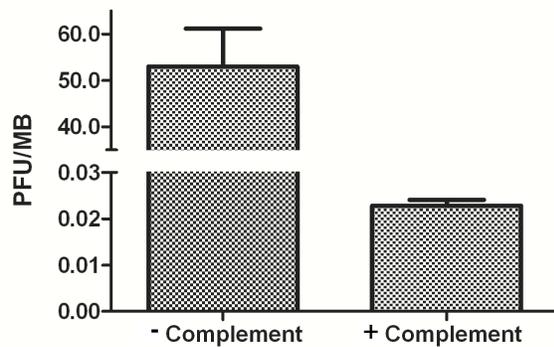
Figure 8. Number of functional Ad particles per microbubble. Complement was used to inactivate unencapsulated and partially encapsulated adenovirus following microbubble packaging.

d. Biodistribution of packaged microbubbles: Microbubble packaged, radioactive Ad particles will be systemically injected into xenograft animal model (65 athymic nude mice) followed by ultrasound and biodistribution analysis to evaluate Ad fate determination. *(Months 15-18)*

Accomplishment. Radiolabeled P-selectin targeted MBs were significantly higher in tumor tissue, as compared with adjacent skeletal tissue or tumor retention of radiolabeled IgG-control-MB (Figure 9, from Warram et al manuscript).
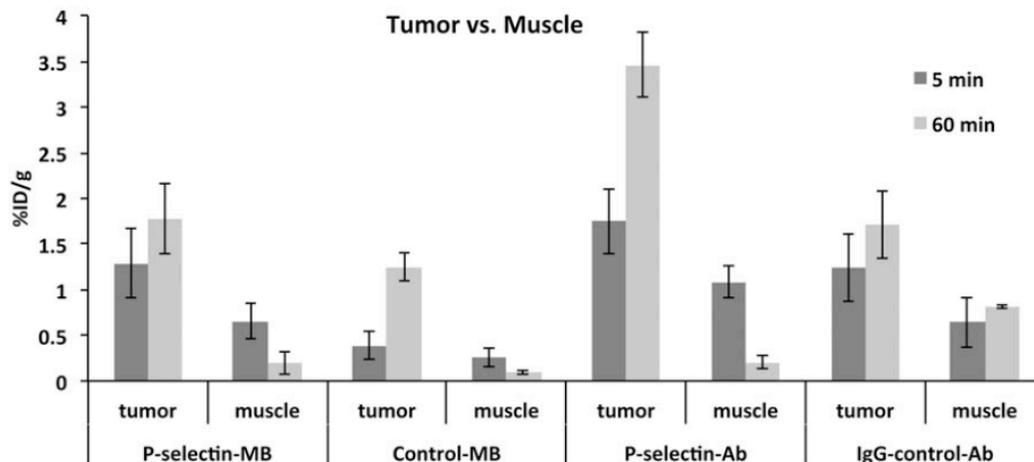
Figure 9. Comparison of percent injected dose per gram (%ID/g) values in tumor and muscle tissue at 5 min and 60 min P-selectin targeted microbubbles (MB), IgG targeted control MB, P-selectin antibody and IgG control groups. Data are means +/- SD.

Task 3: Specific Aim #3: Determine the efficacy of the diagnostic vector combined with the US delivery system to detect malignant prostate cancer. *(Start month 18 and continue to month 36)*

a. In vivo analysis of diagnostic vector in xenograft animal model (30 athymic nude mice) to determine detection sensitivity. *(Months 18-24)*

Accomplishment. SEAP and mCherry levels with the diagnostic Ad in animal models showed excellent correlation of both signals with cancer aggressiveness. Extensive animal experiments were conducted during year 2 to augment preliminary studies in year 1, and the mCherry imaging and SEAP data from year 2 experiments were added to the manuscript that was published in 2014 (Richter et al, Gene Therapy, 2014)

To evaluate the potential of the vector to diagnose prostate cancer in vivo, flank tumors were formed using three different prostate cancer cell lines with low (LNCaP), moderate (PC3) and high (Du145) expression levels of Id1. At the time of vector injection, there were no significant differences in tumor size between any of the groups (LNCaP: $207 \pm 32mm3$; PC3: $203 \pm 37mm3$; Du145: $171 \pm 29mm3$). Elevated plasma levels of PSA were detected in mice bearing LNCaP tumors (1860 ± 144 pg/ml), whereas mice with PC3 and Du145 tumors did not have detectable amounts of PSA. SEAP and mCherry reporter expression were monitored in all mice over a 14-day time period (Figures 10a and 11a). For SEAP analyses, post-treatment levels were compared with baseline SEAP expression measured at day 0 prior to vector injection. Two days after intra-tumoral (IT) injection of Ad5/3-Id1-SEAP-Id1-mCherry, SEAP reporter expression was significantly elevated over baseline levels for the Du145 group, and mCherry reporter fluorescence permitted visual localization of these tumors. SEAP reporter expression was detectable in mice bearing PC3 tumors beginning 2 days after IT injection, and tumor fluorescence was detected at day 6. Post-treatment SEAP levels in mice with LNCaP tumors were slightly elevated above baseline levels beginning at day 6, and mCherry fluorescence was not observed in these tumors at any time point. The SEAP measured in plasma over the entire 14-day time course following vector injection was totaled to represent the effect of making multiple post-treatment diagnostic readings (Figure 10b). The combined effect of successive SEAP measurements revealed an elevated post-treatment SEAP level for each of the tumor types that was significantly greater than the baseline level. Furthermore, a proportional relationship between total amount of measured SEAP and tumor Id1 was observed, with tumors formed by Du145 cells leading to the highest plasma levels of the SEAP reporter and LNCaP tumors having the least. This trend was also observed with mCherry reporter expression, as Du145 tumors had the brightest tumor fluorescence at all time points followed by PC3 tumors and finally LNCaP tumors, which showed negligible mCherry expression (Figure 11). A representative image of the tumor fluorescence visualized at day 6 post vector injection is shown in Figure 11b.
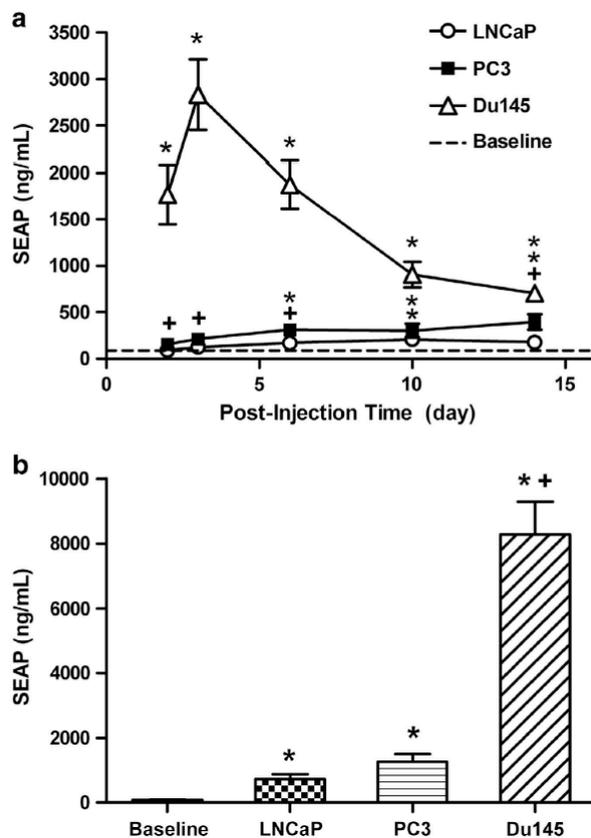
Figure 10. In vivo SEAP reporter expression following IT injection of the diagnostic vector. (a) Plasma levels of the SEAP reporter were monitored over a 14-day period for tumors formed by prostate cancer cells with high (Du145), moderate (PC3) and low (LNCaP) levels of Id1. All data are reported as mean ±s.e.m. (n =5). *P<0.001 vs baseline and +P<0.01 vs baseline (the order of stacked symbols correspond to order of data points). (b) SEAP amounts measured over the entire time course were totaled and compared with baseline levels measured before vector injection. *P<0.001 vs baseline and +P<0.001 vs LNCaP and PC3.
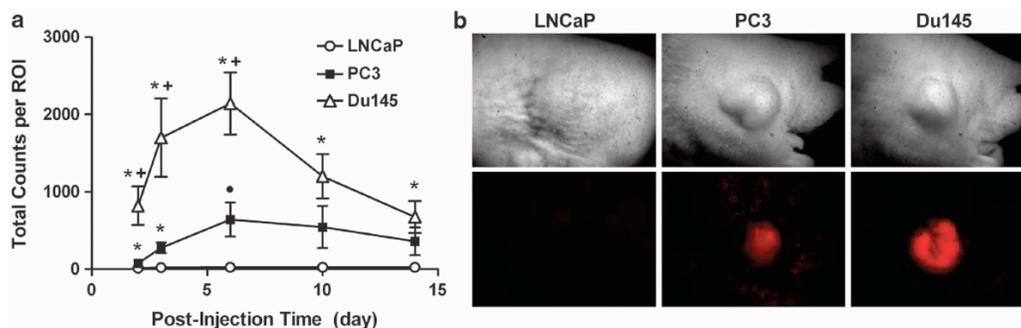
Figure 11. mCherry tumor fluorescence following IT injection of the diagnostic vector. (a) mCherry reporter expression for tumors formed by prostate cancer cells with high (Du145), moderate (PC3) and low (LNCaP) levels of Id1 was monitored and quantified over a 14-day time period. All data are reported as mean ±s.e.m. (n=5). $+p<0.05$ vs PC3; $*p<0.01$ vs LNCaP; $\bullet p<0.05$ vs LNCaP. (b) Representative images of mCherry fluorescence at day 6 post IT injection of the diagnostic vector for LNCaP, PC3 and Du145 tumors. The other task 3 objectives were scheduled for year 3 of the funding period.

Accomplishment: Ultrasound treatment improved Ad-mediated delivery of reporters to PC3 tumors.

Figure 12 shows representative bioluminescence images illustrating enhancement of infectivity at 48 h in the tumors subjected to US-stimulated therapy, as compared with contralateral control tumors and baseline images. Right tumors did not receive US stimulation, while left tumors did.
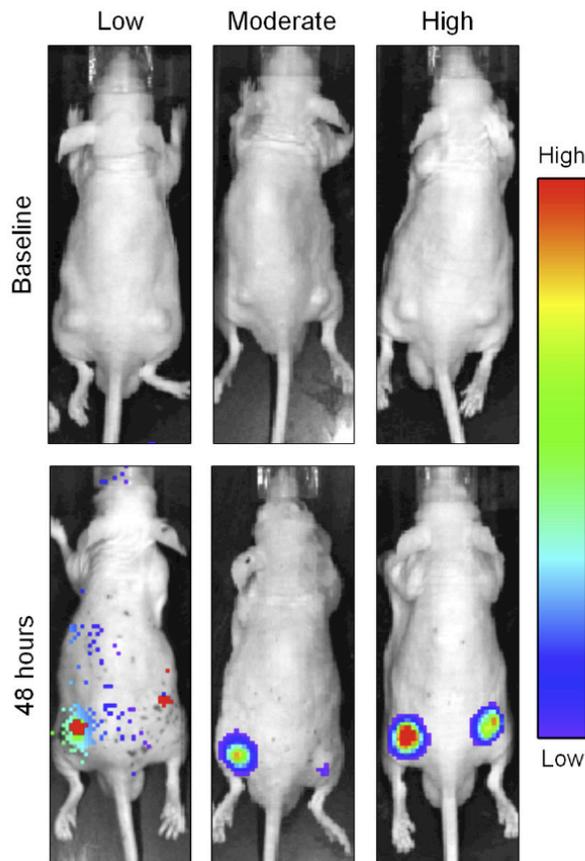
Figure 12. Baseline and 48-post treatment images for mice with PC3 tumors. Left tumors were provided US stimulation.

The other task 3 objectives were for year 3 of the funding period.

4. Key Research Accomplishments:

➢ We evaluated ID1 expression in a panel of prostate cancer cell lines.

➢ We identified differences in Ad infectivity of prostate cancer cell lines, which could be used to normalize the cell lines for comparisons.

➢ Unlike measurements of PSA, which showed no correlation with cellular Id1, expression of the blood-based SEAP reporter showed a significant correlation with prostate cancer cell aggressiveness.

➢ We demonstrated that ultrasound did not change Ad infectivity.

➢ We visualized microbubbles packaged with fluorescently-labeled Ad particles

➢ We quantified the amount of microbubbles with encapsulated Ad and determined the functionality of the Ad particles in complement inactivated microbubbles

➢ We demonstrated that ultrasound with microbubbles improved Ad infectivity in a prostate cancer model (manuscript published, Sorace et al 2013).

➢ SEAP and mCherry levels with the diagnostic Ad in animal models showed excellent correlation of both signals with cancer aggressiveness.

5. Conclusions:

In year 2, a dual reporter vector, Ad5/3-Id1-SEAP-Id1-mCherry, was evaluated for its ability to noninvasively detect and monitor prostate cancer using expression of a SEAP reporter for blood-based detection and mCherry reporter for fluorescence imaging. Reporter expression of the diagnostic system was driven by the cancer-specific expression of Id1, which is a documented indicator of tumor malignancy with no expression found in BPH and normal prostate. Detection of prostate-specific antigen (PSA) as a screening strategy for prostate cancer is limited by the inability of the PSA test to differentiate between malignant cancer and benign hyperplasia. Here, we report the use of a cancer-specific promoter, inhibition of differentiation-1 (Id1), to drive a dual-reporter system (Ad5/3-Id1-SEAP-Id1-mCherry) designed for detection of prostate cancer using a blood-based reporter-secreted embryonic alkaline phosphatase (SEAP) and tumor visualization using a fluorescent reporter protein, mCherry. In human prostate tumors, Id1 levels are correlated with increased Gleason grade and disease progression. To evaluate in vivo performance, flank tumors were grown in athymic male mice using three prostate cancer cell lines. Following intra-tumoral injection of the vector, tumors formed by cells with high Id1 had the greatest reporter expression. Interestingly, tumors with the lowest levels of Id1 and reporter expression produced the greatest amounts of PSA. These data support the use of Ad5/3-Id1-SEAP-Id1-mCherry as a predictor of prostate cancer malignancy and as a strategy for tumor localization.

The dependency of the diagnostic vector on adequate expression of Id1 represents a limitation of the current system for detecting less aggressive cancers. However, by achieving targeted delivery and increased tumor infectivity, the visual detection limits of the diagnostic vector can be surpassed. Our future work will aim to develop strategies to target vector delivery and infectivity of both aggressive and non-aggressive prostate cancer to allow for sensitive localization to aid in tumor resection. In the past year we have discussed localized delivery to the prostate of the diagnostic vector with interventional radiology approaches.

In conclusion, the present work introduces a novel strategy for detection and localization of prostate cancer that overcomes the current limitations of the PSA test to distinguish between aggressive cancer and indolent conditions like BPH. The correlation between reporter expression and cellular Id1 enables SEAP levels to be used as a predictive measure of prostate cancer aggressiveness and mCherry fluorescence as an aid for tumor visualization. This strategy would assist clinicians in the detection and treatment of prostate cancer and ultimately reduce the mortality associated with this disease.

6. Publications, Abstracts, and Presentations
a. List all manuscripts submitted

1. Lay Press: none

2. Peer-reviewed scientific journals published:
1. Sorace AG, Warram JM, Mahoney M, Zinn KR, Hoyt K. Enhancement of adenovirus delivery after ultrasound-stimulated therapy in a cancer model. Ultrasound in Medicine and Biology, 39: 2374-2381, 2013. NIHMSID: 574284
2. Warram JM, Sorace AG, Mahoney M, Samuel S, Harbin B, Joshi M, Martin A, Whitworth L, Hoyt K, Zinn KR. Biodistribution of P-selectin targeted microbubbles. Journal of Drug Targeting, 22: 387-394, 2014.
3. Hoyt K, Mahoney M, Sorace AG. Four-dimensional molecular ultrasound imaging of tumor angiogenesis in a preclinical animal model of prostate cancer. IEEE International Ultrasonics Symposium Proceedings, 1:1-4, 2014.
4. Richter JR, Mahoney M, Warram JM, Samuel S, Zinn KR. A Dual-Reporter, Diagnostic Vector for Detection and Localization of Prostate Cancer, Gene Ther (published online 7/24/14)

3. Invited: none

4. Abstracts Published:

1. Sorace AG, Mahoney M, Zinn KR, **Hoyt K**. Volumetric molecular ultrasound imaging of tumor vascularity in a preclinical model of prostate cancer. American Institute for Ultrasound in Medicine Annual Convention, 32:S16, 2013.

b. Presentations:

1. Sorace AG, Mahoney M, Zinn KR, Hoyt K. Volumetric molecular ultrasound imaging of tumor vascularity in a preclinical model of prostate cancer. American Institute for Ultrasound in Medicine Annual Convention, 32:S16, 2013.
2. Sorace AG, Warram JM, Mahoney M, Zinn KR, Hoyt K. Ultrasound-stimulated gene therapy for improved adenovirus infection. World Molecular Imaging Congress, 2013.
3. Warram JM, Sorace AG, Mahoney M, Samuel S, Harbin B, Joshi M, Martin A, Whitworth L, Hoyt K, Zinn KR. Biodistribution of P-selectin targeted microbubbles. World Molecular Imaging Congress, 2013.
4. Hoyt K, Sorace AG, Mahoney M, Zinn KR. Detection of prostate tumor angiogenesis by volumetric molecular ultrasound imaging in an animal model. World Molecular Imaging Congress, 2013.
5. Hoyt K. Molecular imaging. American Institute for Ultrasound in Medicine Annual Convention, 33:S45, 2014 (Invited).
6. Sorace AG, Warram JM, Mahoney M, Zinn KR, Hoyt K. Ultrasound-stimulated gene therapy for improved adenovirus delivery. American Institute for Ultrasound in Medicine Annual Convention, 33:S54, 2014.
7. Hoyt K, Mahoney M, Sorace AG. Four-dimensional molecular ultrasound imaging of tumor angiogenesis in a preclinical animal model of prostate cancer. IEEE International Ultrasonics Symposium, 2014.
8. Warram JM, Mahoney M, Zinn KR. "Combined imaging and screening of prostate cancer." *2013 World Molecular Imaging Congress.* Savannah, Georgia. 2013.
9. Richter JR, Mahoney M, Warram JM, Samuel S, Zinn KR. "A dual-reporter, diagnostic vector for detection and localization of prostate cancer." *2013 UAB Comprehensive Cancer Center Retreat.* Birmingham, Alabama. 2013.

7. Inventions, Patents and Licenses
nothing to report

8. Reportable outcomes
We report the development of dual reporter vector, Ad5/3-Id1-SEAP-Id1-mCherry, that can be used as a tool for combined blood-based screening with imaging for detection of aggressive prostate cancer.

9. Other Achievements

Degree Awarded
M.S. degree to Marshall Mahoney

Employment or research opportunities applied for and/or received based on experience/training supported by this award.
Dr. Jason Warram was hired as an Instructor in the UAB Department of Surgery, effective Oct. 1, 2013

Personnel supported by this grant:

Dr. Kurt R. Zinn, PI

Dr. Kenneth Hoyt
Dr. Jason Warram (post-doctoral fellow, taking faculty position at UAB in Oct. 2013)
Dr. Jill Richter (post-doctoral fellow, recruited to take Dr. Warram's position on the grant)
Dr. Sudarshan
Marshall Mahoney (M.S. student, graduated in May 2013 with M.S. degree)
Sharon Samuel

10. References:

1. Sorace AG, Warram JM, Mahoney M, Zinn KR, **Hoyt K**. Enhancement of adenovirus delivery after ultrasound-stimulated therapy in a cancer model. Ultrasound in Medicine and Biology, 2013
2. Sorace AG, Mahoney M, Zinn KR, **Hoyt K**. Volumetric molecular ultrasound imaging of tumor vascularity in a preclinical model of prostate cancer. American Institute for Ultrasound in Medicine Annual Convention, 32:S16, 2013.

11. Appendices:

1. Sorace AG, Warram JM, Mahoney M, Zinn KR, Hoyt K. Enhancement of adenovirus delivery after ultrasound-stimulated therapy in a cancer model. Ultrasound in Medicine and Biology, 39: 2374-2381, 2013. NIHMSID: 574284
2. Warram JM, Sorace AG, Mahoney M, Samuel S, Harbin B, Joshi M, Martin A, Whitworth L, Hoyt K, Zinn KR. Biodistribution of P-selectin targeted microbubbles. Journal of Drug Targeting, 22: 387-394, 2014.
3. Hoyt K, Mahoney M, Sorace AG. Four-dimensional molecular ultrasound imaging of tumor angiogenesis in a preclinical animal model of prostate cancer. IEEE International Ultrasonics Symposium Proceedings, 1:1-4, 2014.
4. Richter JR, Mahoney M, Warram JM, Samuel S, Zinn KR. A Dual-Reporter, Diagnostic Vector for Detection and Localization of Prostate Cancer, Gene Ther (published online 7/24/14)

ELSEVIER

● *Original Contribution*

ENHANCEMENT OF ADENOVIRUS DELIVERY AFTER ULTRASOUND-STIMULATED THERAPY IN A CANCER MODEL

Anna G. Sorace,* Jason M. Warram,[†] Marshall Mahoney,* Kurt R. Zinn,*[†‡§]
and Kenneth Hoyt*[†‡§]

*Department of Biomedical Engineering, University of Alabama at Birmingham, Birmingham, Alabama, USA; [†]Department
of Radiology, University of Alabama at Birmingham, Birmingham, Alabama, USA; [‡]Department of Electrical & Computer
Engineering, University of Alabama at Birmingham, Birmingham, Alabama, USA; and [§]Comprehensive Cancer Center,
University of Alabama at Birmingham, Birmingham, Alabama, USA

Abstract—Improving the efficiency of adenovirus (Ad) delivery to target tissues has the potential to advance the translation of cancer gene therapy. Ultrasound (US)-stimulated therapy uses microbubbles (MBs) exposed to low-intensity US energy to improve localized delivery. We hypothesize that US-stimulated gene therapy can improve Ad infection in a primary prostate tumor through enhanced tumor uptake and retention of the Ad vector. *In vitro* studies were performed to analyze the degree of Ad infectivity after application of US-stimulated gene therapy. A luciferase-based Ad on a ubiquitous cytomegalovirus (CMV) promoter (Ad5/3-CMV-Luc) was used in an animal model of prostate cancer (bilateral tumor growth) to evaluate Ad transduction efficiency after US-stimulated therapy. Bioluminescence imaging was employed for *in vivo* analysis to quantify Ad infection within the tumor. *In vitro* studies revealed no difference in Ad transduction between groups receiving US-stimulated therapy using high, low or sham US intensity exposures at various multiplicities of infection (MOIs) ($p = 0.80$). *In vivo* results indicated that tumors receiving US-stimulated therapy after intra-tumoral injection of Ad5/3-CMV-Luc (1×10^6 plaque-forming units) exhibited a 95.1% enhancement in tumor delivery compared with control tumors receiving sham US ($p = 0.03$). US-stimulated therapy has significant potential to immediately affect Ad-based cancer gene therapy by improving virus bioavailability in target tissues. (E-mail: hoyt@uab.edu)   © 2013 World Federation for Ultrasound in Medicine & Biology.

Key Words: Cancer, Gene therapy, Microbubble contrast agent, Ultrasound, Adenovirus, Transduction.

INTRODUCTION

There is an urgent need to improve delivery of recombinant adenovirus (Ad) to advance cancer gene therapy. Ad vectors have immense potential in cancer therapy because of their ability to infect tumor cells while not injuring healthy tissue. Multiple applications using Ad vectors in cancer have been explored. Therapeutic strategies often involve the triggering of cell death *via* a death-inducing reporter that is specifically driven by a cancer promoter (Choi et al. 2012). Other utilities involve immunotherapeutic approaches aimed at inducing host anti-tumor immune responses (Lupold and Rodriguez 2005). Direct cancer cell death can be accomplished through delivery of replication oncolytic viruses or non-replicating vectors encoding tumor suppressor genes, suicide genes or anti-angiogenic genes (Kaplan 2005). Tumor cells can be destroyed at both primary and metastatic locations through induction of host anti-tumor immune responses. Although gene therapy has advanced in the last decade, there are many limitations that prevent routine applications. The effectiveness of gene therapy is directly dependent on successful site-specific delivery (Choi et al. 2013). Limitations of delivery include anti-Ad host immune response, inadequate efficiency of tumor cell transduction and extravasation of the large molecules to their intended site; in addition, the ubiquitous Ad receptor can lead to virus uptake in cell types other than the targeted region (Choi et al. 2012; Fukazawa et al. 2010; Yun 2013). Additional hurdles include the inability to overcome filtration from the liver and the limited infectivity of Ad serotype 5 (Ad5). These limitations lead to necessary advancements in the field of Ad delivery.

Address correspondence to: Kenneth Hoyt, University of Alabama at Birmingham, Volker Hall G082, 1670 University Boulevard, Birmingham, AL 35294, USA. E-mail: hoyt@uab.edu

Ultrasound (US)-stimulated therapy provides a localized technique to enhance agent delivery. Micro-bubbles (MBs) are clinically used US contrast agents and have proven to be non-immunogenic and non-toxic in nature (Calliada et al. 1998; Cosgrove 2006). In this unique therapy, US-exposed MBs both increase cell membrane permeability and induce localized molecular extravasation (Dijkmans et al. 2004; Ferrara et al. 2007; Lindner et al. 2004; Song et al. 2002; Sorace et al. 2012b). Although there is some evidence disputing the exact duration of this effect, this therapeutic stimulation has been shown to last up to 30 min post-US exposure (Sorace et al. 2013). Depending on the US setup and vari-ance between US parameters used for US therapy, differ-ences in sustained permeability have been found on the order of minutes to hours, and there have even been permanent non-reversible reactions (Böhmer et al. 2010; Caskey et al. 2009; Chin et al. 2009; Stieger et al. 2007; Tamosiūnas et al. 2012). US-stimulated therapy has been increasingly popular in pre-clinical models because it is generally non-invasive and has significant potential for translation. US-stimulated therapy has been found to increase delivery of cytotoxic agents to cancer cells and to improve response by greater than 50% compared with drug alone (Casey et al. 2010; Heath et al. 2012; Sorace et al. 2012b). It has also been found that positive effects can be achieved after only a single dose (Sorace et al. 2013). Other applications of this therapy include delivery of drugs through the blood–brain barrier and enhancement of delivery of DNA (Klibanov 2006; McDannold et al. 2012; Sirsi and Borden 2012; Treat et al. 2012). Studies have also indicated that Ad particles can be safely delivered to a localized region by MB packaging to avoid ubiquitous uptake in other cells and liver filtration (Howard et al. 2006; Warram et al. 2012). Improvement of gene delivery through increased extravasation can occur by displacing endothelial cells and improving pathways for delivery. Thus, US exposure is a good adjuvant treatment for standard gene and drug delivery. Ultrasonic techniques have been explored as an application in gene delivery through heat-sensitive lipo-somes and head shock protein promoters. This approach allows for a triggered release after elevating the tissue temperature with US (Frenkel 2008). Another US-based approach to gene delivery is pre-treatment with pulsed high-intensity focused ultrasound, which allows for increased extravasation. In particular, high-intensity focused ultrasound has been found to be a positive treat-ment in addition to targeted antibody therapy plus adeno-virus delivery, resulting in improved tumor regression (Patel et al. 2007). US-stimulated gene delivery using mi-crobubble cavitation and low-intensity fields has recently been explored to improve oncolytic virus transduction

and was found to improve tumor uptake analysis without damaging surrounding tissue (Bazan-Peregrino et al. 2013). To the best of our knowledge, applying MBs and low-intensity US-stimulated therapy to enhance a ubiqui-tous Ad for tumor delivery is a novel application of this US technology.

To establish genetic-based therapeutics as a routine treatment option for cancer patients, delivery barriers must be overcome (de Vrij et al. 2010). In the study described here, US-stimulated therapy was evaluated for its potential to improve Ad vector transduction in an animal model of prostate cancer. Considering the relative tolerability of US-stimulated therapy, positive evaluation of this technique could immediately affect Ad-based therapy trials, leading to improved treatment success and patient survival.

METHODS

Adenovirus preparation

A non-replicative, luciferase reporter-based, sero-type 5 Ad on a ubiquitous cytomegalovirus (CMV) promoter (Ad5/3-CMV-Luc) was used to evaluate Ad transduction because of the ease of bioluminescence imaging for evaluation of response. To improve infec-tivity by eliminating Coxsackie Ad receptor-mediated infection, the Ad5/3-CMV-Luc contains a chimeric infec-tivity motif that consists of an Ad serotype 3 knob on an Ad serotype 5 fiber (Borovjagin et al. 2005). For the study, particles were amplified in HEK-293 cells and purified using cesium chloride centrifugation gradients. A standard agarose-overlay plaque assay was conducted with HEK-293 cells to determine a viral titer of 1.1×10^{11} plaque-forming units (PFU) per milliliter.

Cell culture

PC3 human prostate cancer cells were purchased from the American Tissue Type Collection (Manassas, VA, USA). The cell line was maintained in Dulbecco's modified Eagle medium (DMEM) with 10% fetal bovine serum and 1% L-glutamine. All cells were grown to 80% to 90% confluence before passaging. Cell numbers were determined using a standard hemocytometer, and cell viability was measured by trypan blue dye exclusion.

In vitro experimentation

Experiment 1. Aliquots (0.1 mL in phosphate-buffered saline [PBS]) of Ad5/3-CMV-Luc were placed in 1.5-mL polypropylene micro-centrifuge tubes at various PFU amounts (0, 3.5, 3.5×10^1, 3.5×10^2 and 3.5×10^3 infectious virus particles). Groups were then subdivided into low-pressure US, high-pressure US and sham US exposure (control) groups. All groups were evaluated in triplicate. To each tube, 10 μL of MBs (total

of 9.3×10^7 MBs, Definity, Lantheus Medical Imaging, North Billerica, MA, USA) was added immediately before US-stimulated therapy. Groups were exposed to US in a 37°C water bath with the following acoustic parameters: transmit frequency = 1.0 MHz, peak negative pressures = 0.85 MPa (higher-pressure condition) or 0.1 MPa (low-pressure condition), pulse repetition period = 0.1 s, 10% duty cycle = 10%, duration of US exposure = 5 min. An unfocused, single-element (0.75-in.) immersion transducer (Olympus, Waltham, MA, USA) was placed in series with a signal generator (AFG3002 B, Tektronix, Beaverton, OR, USA) and power amplifier (A075, Electronics and Innovation, Rochester, NY, USA). US intensity measurements were performed in a 37°C water bath using a hydrophone (Model HGL-0400, ONDA, Sunnyvale, CA) and pre-amplifier setup in series with a digital oscilloscope for voltage signal monitoring and recording. The immersed transducer was manipulated with a precision stepper motor (Velmex, Bloomfield, NY, USA) to locate the spatial peak pressure maximum. Peak negative pressure measurements were determined by converting voltage to pressure measurements using hydrophone calibration data. Tumor and cell samples were placed in the near field.

Adenovirus groups were then added at various multiplicities of infection (MOIs) (0, 0.01, 0.1, 1, and 10) to PC3 cells (3.5×10^2 cells per well in a 24-black-well plate) plated 24 h earlier. Note that an MOI value is defined as the ratio of Ad particles to infectious targets (*i.e.,* number of cells per well). Virus aliquots were allowed to incubate for 1 h and were then removed and replaced with complete medium. After a 24-h incubation period (after Ad vector exposure), luciferin was added and bioluminescence imaging completed. Luciferin (2.5 mg, Caliper Life Sciences, Hopkinton, MA, USA) was diluted into 25 mL of PBS. Medium was removed from the plates and replaced with 1 mL of diluted luciferin (100 μg) per well to over-saturate the cells. Bioluminescence imaging was performed using the IVIS-100 System (Xenogen, Hopkinton, MA, USA) with an image acquisition time of 300 s (binning of 8 and f/stop of 1) at a fixed stage height. Exposure time was chosen to heighten the signal, while avoiding over-saturation. A region of interest was drawn around each well, and the bioluminescence signal was summarized as total photon counts using equipment software (Living Image 4.2, Xenogen).

Experiment 2. Aliquots (0.1 mL in PBS) of PC3 cells (3.5×10^2) and Ad5/3-CMV-Luc (3.5×10^2 PFU, MOI = 1) in polypropylene micro-centrifuge tubes underwent high-pressure US treatment ($N = 13$) or sham US treatment ($N = 13$) in the presence of MBs in a 37°C water bath using the same high-pressure US parameters used in experiment 1. After US therapy, cells

and Ad were plated in a 24-well plate and then rinsed and replaced with complete medium after 1 h. Twenty-four hours later, plates were imaged for the presence of bioluminescence as described in the previous section.

In vivo experimentation

Animal studies were approved by the Institute of Animal Care and Use Committee at the University of Alabama at Birmingham. PC3 cancer cells (2×10^6 cells per 100 μL DMEM without fetal bovine serum) were implanted subcutaneously into the left and right flanks of 5-wk-old nude athymic male mice (Frederick Cancer Research, Hartford, CT, USA) ($N = 24$ animals, $N = 48$ tumors). Tumors were allowed to grow approximately 5 wk to equal tumor size according to caliper measurements (final tumor size = 34.1 ± 2.8 mm^2). Each animal received a 30-μL (2.8×10^8 MBs) tail vein injection of MBs (Definity) diluted to a final volume of 100 μL with saline. Animals were then submerged in a custom-built 37°C water bath and remained under isoflurane gas anesthesia for the entire US-stimulated therapy. Two minutes after MB injection, the left flank tumor was exposed to US (at the higher pressure in to these experiments, 0.85 MPa). Right flank tumors were not exposed to US. US-stimulated therapy was administered using the previously detailed parameters. This setup allowed exposure of the entire target tumor to US energy while the contralateral tumor was outside the path of US transmission. Immediately after US, the Ad5/3-CMV-Luc vector was injected intra-tumorally into both the left and right flank tumors. Animals were divided into three groups and administered different Ad concentrations: 1×10^6 PFU ($N = 12$), 1×10^7 PFU ($N = 5$) and 1×10^9 PFU ($N = 7$), which, for the remainder of this article, are referred to as the "low," "medium" and "high" concentrations of Ad, respectively. Intratumoral doses were administered in a total volume of 50 μL. Animals were imaged for bioluminescence expression before therapy on day 0 (baseline) and again on day 2 (48 h post-therapy) using the following methods. Animals were injected intra-peritoneally with firefly luciferin (2.5 mg), which is catalyzed by luciferase to produce a bioluminescence reporter signal after luciferase gene expression. After a 15-min period allowing for systemic circulation, all animals were oriented so both tumors were visualized and then imaged for bioluminescence expression using the IVIS-100 system (Xenogen Corporation) and established data acquisition protocols. Five animals were imaged simultaneously using a 300-s exposure, f/stop of 1, binning of 8 and fixed stage height. Standardized regions of interest were generated using instrument software to analyze photon counts. Day 0 was used as background signal and was subtracted from the day 2 signals.
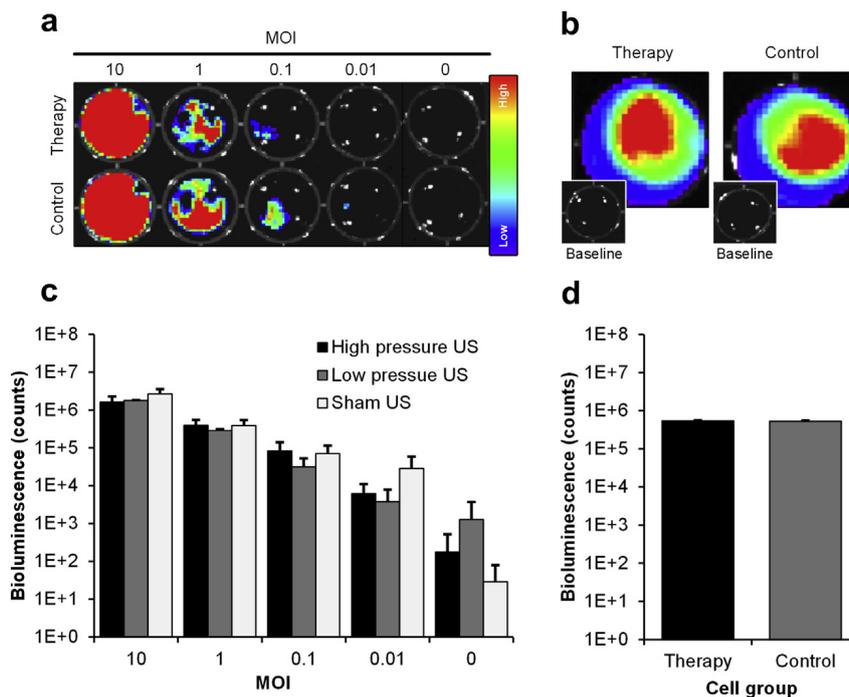
Fig. 1. Representative bioluminescence images of plated cancer cells incubated with adenovirus (Ad) vectors after exposure to high-pressure ultrasound (US)-stimulated therapy or sham (control) US (a). Detailed analysis of the bioluminescence signal (counts) representing Ad infection efficiency after the Ad vector was exposed to acoustic conditions akin to those used during US-stimulated therapy (c). Sham or US exposure at low or high acoustic pressures did not produce any differential effects on or alterations in Ad infectivity potential. US-stimulated therapy of cancer cell cultures incubated with an Ad vector resulted in no significant differences in bioluminescence images (b) or Ad infectivity rates (d), which again indicates US had no negative effects on Ad vector infectivity or the transduction pathway. Illustrated here are means ± standard errors of the means. MOI = multiplicity of infection.

Statistical analysis

All experimental data were expressed as means ± standard errors of the mean and reported as percentage change or bioluminescence count. Analysis of variance was completed to assess differences within *in vitro* data in experiment 1. An unpaired, two-sample *t*-test was used to measure differences in US-stimulated and control cell groups within *in vitro* data in experiment 2. A two-sample paired *t*-test was used to calculate statistical differences between control and US-stimulated tumors within each group. No direct comparisons were made between the various Ad concentration groups. A *p*-value less than 0.05 was considered to indicate statistical significance. Analyses were completed using the SAS statistical software package (Cary, NC, USA).

RESULTS

During *in vitro* experiment 1, various concentrations of Ad particles were subjected to US-stimulated therapy in the absence of cells to determine the effect of US treatment on the infectivity potential of the virus. After US exposure, the Ad was added to plated cells at various MOIs and allowed in incubate. Bioluminescence imaging

resulting from successful Ad infection revealed that there is no significant difference in virus infectivity or vector transduction between exposures to high, low or no (sham) US pressures ($p = 0.80$) (Fig. 1a, c). Only control and high-pressure therapy are illustrated, as exposure to low pressure also results in no qualitative or quantitative differences. The importance of this finding is that it confirms that exposure of the Ad vector to the US intensity levels necessary for inducing membrane permeabilization during US-stimulated therapy has no negative effect on the infectivity potential of the Ad. The various MOIs tested confirm that this observation was consistent across various concentrations of Ad.

For *in vitro* experiment 2, Ad particles were subjected to US-stimulated therapy in the presence of PC3 cells (MOI = 1) to determine the effects of US treatment on cellular response to infection. The control group contained Ad5/3-CMV-Luc, cancer cells and MBs without US treatment. Figure 1b and d illustrate that there was no difference in bioluminescence expression after Ad infection between the therapy group ($5.4 \times 10^5 \pm 1.9 \times 10^4$ counts) and the control group ($5.3 \times 10^5 \pm 2.0 \times 10^4$ counts) ($p = 0.92$). These results suggest that there was no cellular internalization of the

Ad. US-stimulated therapy had neither negative nor positive effects when applied to a combination of MBs, cells and Ad.

Ultrasound-stimulated gene therapy effects on Ad5/3-CMV-Luc transduction in an *in vivo* model of prostate cancer were also analyzed. Bilateral flank tumors were to provide *in situ* control tumors that did were not exposed to US. After US-stimulated therapy of treatment tumors, Ad5/3-CMV-Luc was immediately administered to the three animal groups *via* an intra-tumoral injection using low, moderate and high concentrations of Ad. Forty-eight hours after treatment, the low concentration therapy group had a 95.1 ± 35.1% increase in bioluminescence expression compared with the control group ($p = 0.03$). At the moderate concentration, the therapy group exhibited a 12.1 ± 6.4% increase compared with the control, trending toward significance ($p = 0.06$). Finally, at the high concentration, the therapy group exhibited no difference (10.1 ± 22.8% increase) compared with the control group ($p = 0.09$) (Fig. 2a). The average photon/second tumor expressions for the different concentrations are (therapy) and 157.1 (control) for low, 629.1 (therapy) and 546.8 (control) for moderate and 212,877.9 (therapy) and 154,899 (control) for high. Qualitative analysis revealed the visual differences in overall bioluminescence expression between treated and control tumors receiving low, moderate and high Ad concentrations, at baseline and 48 h. Figure 2b comprises representative bioluminescence images illustrating enhancement of infectivity at 48 h in the tumors subjected to US-stimulated therapy, as compared with contralateral control tumors and baseline images. Further analysis of the low Ad concentration group revealed that at baseline, there were no statistical significant differences between control tumors and tumors subjected to US therapy ($p = 0.27$). Individual analysis of the animals in the group administered the low concentration of Ad indicates that in 75% of the animals infectivity increased, and in 17% there was relatively no change (which is defined as less than 20% change as compared with the control); one animal had a negative response (Fig. 3).

DISCUSSION

Enhanced tissue-specific delivery of Ad-based vectors has the potential to significantly improve current cancer gene therapy protocols. The strategies investigated here represent original advances in delivery of Ad to intended regions to improve virus transduction within the target tumor tissue. The *in vitro* studies confirmed that Ad infectivity was not affected by either the high or low US pressure condition (frequency = 1.0 MHz). Although in the approach used in this study the virus was injected after US-stimulated therapy, evaluation of
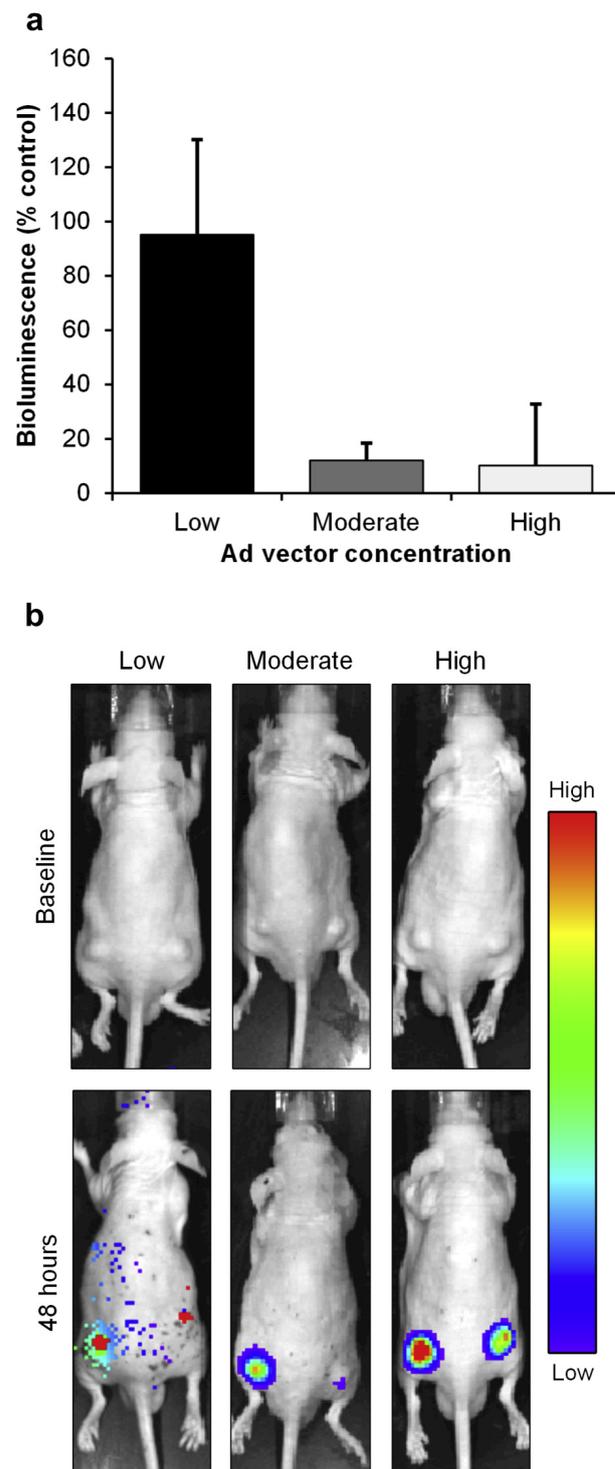
Fig. 2. Ultrasound (US)-stimulated therapy improves delivery of the adenovirus (Ad) vector to target flank tumors, especially at low Ad concentrations (a). Representative bioluminescence images at baseline and 48 h after US-stimulated therapy for various Ad concentrations denoted as low, moderate and high (b). US-stimulated therapy produced an increase in bioluminescence signal measurements (*via* increased Ad infection) over contralateral control tumors at various Ad concentrations. Illustrated here are means ± standard errors of the means.
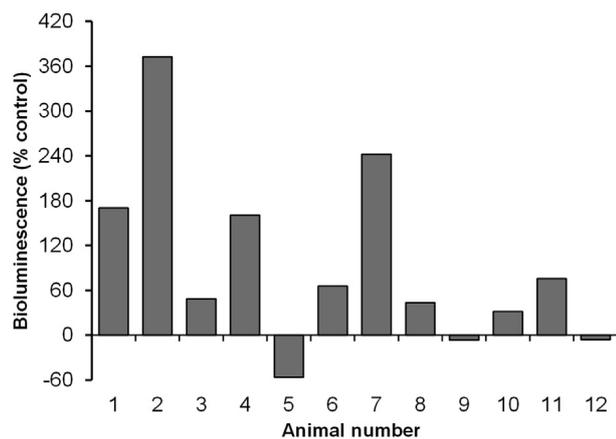
Fig. 3. Analysis of individual animals in the low adenovirus (Ad) concentration group, which exhibited the greatest enhancement after ultrasound (US)-stimulated therapy. Of the animals investigated, 75% of the tumors produced increased bioluminescence signals compared with contralateral tumors. These findings were attributed to improved Ad retention and infectivity in the target tumor receiving US-stimulated therapy.

the direct effects of US-stimulated therapy on Ad particles was necessary for future translation and investigations. We can thus be confident that in future studies, administration of multi-dose or intra-tumoral injections before therapy will not alter the gene therapy vector during exposure to the US energy levels detailed in this article. Another limitation of the in *vitro* studies is that there is a difference in the US intensity that reaches the cells *in vitro* and *in vivo* because of the polypropylene tubes that house the cells in suspension. This was also calculated with hydrophone measurements, and adjustments *in vitro* have to be made accordingly to equalize the pressures received. Differences in intensity have been found to decrease by 15%–50% when cells in suspension versus monolayers are analyzed (Sorace et al. 2012a). It is difficult to directly compare *in vitro* and *in vivo* conditions in any study; therefore, assumptions are made.

Internalization of the Ad vector, which ultimately leads to tissue infection, is triggered by interaction of the viral penton with epithelial integrins. From there it is processed to the nucleus and is eventually expressed (Lupold and Rodriguez 2005). The Ad requires receptor-mediated internalization; therefore, intracellular delivery through membrane permeabilization could decrease expression (Greber et al. 1993). *In vitro* experiments indicated that increased Ad transduction did not occur and therefore was not due to increased infection by altering the mechanisms of the adenoviral process or internalization. This is consistent with previous studies analyzing gene transfer with US-stimulated therapy (Miller and Quddus 2000; Price et al. 1998). Bioluminescence signal measurements between *in vitro* experiments indicated the precision of infection at

a MOI of 1. US alone has the capacity to increase the temperature of the surrounding medium, which could potentially alter infection rate; however, there was no change in water bath temperature as monitored throughout each US treatment session. No differences were found in Ad infectivity *in vitro* when US-stimulated therapy was applied directly to cells. Previous experiments had indicated no decreases in cell viability under similar US-stimulated conditions (Sorace et al. 2012b). The MOI of 1 was chosen for this experiment so as not to over-saturate the cells to more accurately evaluate and quantify interactions between cells and Ad. Considering that receptor-mediated internalization is required for successful virus infection, US-induced internalization would not lead to reporter transduction. Therefore, observation of a decrease in bioluminescence signal within the US group would indicate that the viral particles were sequestered inside the cell and not available for traditional infection. Because no such observation was made, it was concluded that US-stimulated internalization did not occur. It is proposed that the large size of the Ad vector compared with drug molecules decreases its ability to be internalized through a membrane permeabilization effect of US-stimulated therapy.

Detailed *in vivo* studies evaluated enhancement of Ad delivery after US-stimulated therapy in an animal model of prostate cancer. US-stimulated therapy is effective because when induced with lower-intensity US parameters, MBs mechanically oscillate and interact with endothelial cells. This massaging mechanism allows for displacement of cells and breaking of gap junctions, allowing further permeability and extravasation into the tumor (Frenkel 2008). The greatest enhancement of Ad transduction was observed at the lowest vector dose, whereas little or no change was observed at the highest doses. At the highest dose, Ad availability at the cancer cell level was not a boundary for transduction because of the high concentration (tissue saturation) of the Ad vector. Considering that the purpose of the study was to highlight enhancement of transduction by US-stimulated therapy, the lowest dose provided the greatest potential for improvement. Although 75% of the animals studied had a positive outcome when administered a low concentration of Ad in combination with US-stimulated therapy, one animal had a decrease in Ad tumor delivery. The negative response in this animal could possibly be the result of poor intra-tumoral injection. An additional source of variation within the group could be the variability between tumor vascularity and differences in necrotic regions within the tumor. Nevertheless, the use of this promising US technology would improve the bioavailability of low Ad vector doses and allow a lower dose to achieve the same therapeutic effect as a high dose. This outcome could help reduce toxic effects in patients,

which currently hinder widespread use of gene therapy techniques in the clinic. As opposed to intra-venous injections, intra-tumoral injections can offset the limitations of adenoviral gene delivery such as the anti-Ad host immune response and the ubiquitous Ad receptor leading to adenoviral uptake in all cell types.

Several studies detailed in the literature have investigated enhancement of gene transfection efficiency with US-stimulated delivery in various tissue types. Specifically, with plasmid DNA integrated into a MB shell, once the injected agents reached the target tumor tissue, high-intensity US energy destroys the MB and triggers localized payload (DNA) delivery (Sirsi et al. 2012). Using bioluminescence imaging techniques, this group was able to determine a significantly higher region of expression within the tumor than in normal tissue. Research analyzing the longitudinal effects of anti-angiogenic gene therapy on hepatocellular carcinoma revealed a significant decrease in micro-vessel density and increase in apoptosis using US-stimulated therapy with plasmid compared with plasmid alone (Nie et al. 2008). Various other studies have investigated US-stimulated delivery of genetic material in the heart (Bekeredjian et al. 2005; Shohet et al. 2000; Tsunoda et al. 2005), pancreas (Chen et al. 2006), skeletal muscle (Wang et al. 2005; Zhang et al. 2006), kidney (Koike et al. 2005), central nervous system (Shimamura et al. 2005) and solid tumors (Nie et al. 2008; Wang et al. 2009; Warram et al. 2012).

Phase I and II trials to evaluate Ad vector delivery in humans are underway. Ad vectors are being explored because of their high transduction efficiency compared with a retrovirus or lentivirus. Phase II clinical studies on Ad-based prostate-specific antigen (PSA) vaccine are also being conducted. The PSA vaccine has been deemed tolerable with minimal toxic effects compared with more conventional anti-cancer drugs, and the investigators hope that the Ad vector will produce immunity to the PSA and destroy cancer cells producing PSA (NCT00583024) (Department of Defense 2007 [cited from 2013]). Along with the vaccines that are being studied, there is also a phase I trial using an Ad5.SSTR/TK.RGD gene therapy vector, which is an infectivity-enhanced Ad that expresses a therapeutic thymidine kinase suicide gene and a somatostatin receptor (SSTR) for imaging patients with recurrent gynecologic cancer. When used in combination with a chemotherapeutic drug (ganciclovir), this novel Ad vector has been found to induce cancer cell apoptosis (Kim et al. 2012). This particular study used an Ad to image gene transfer and monitor therapeutic response and represents one of the first studies of its kind to prove tolerability and efficacy in humans. Notwithstanding, these authors noted that further refinements in enhancing Ad vector infectivity

are needed. Incorporation of US-stimulated gene therapy may help overcome this problem.

The ability to protect Ad vectors from systemic clearance and liver retention while enhancing their bioavailability within the tumor is an important advancement in gene delivery to target tumors. Previous research has indicated that US-stimulated therapy can enhance delivery of both drugs and plasmids for cancer treatment. To the best of our knowledge, this article represents the first study using US-stimulated therapy to improve delivery of Ad to the target tumor. Our result illustrating that Ad infection can be considerably enhanced after a single session of US-stimulated therapy is a significant finding in the field of cancer gene therapy and warrants further investigation.

REFERENCES

Bazan-Peregrino M, Rifai B, Carlisle RC, Choi J, Arvanitis CD, Seymour LW, Coussios CC. Cavitation-enhanced delivery of a replicating oncolytic adenovirus to tumors using focused ultrasound. J Control Release 2013;169:40–47.

Bekeredjian R, Grayburn PA, Shohet RV. Use of ultrasound contrast agents for gene or drug delivery in cardiovascular medicine. J Am Coll Cardiol 2005;45:329–335.

Böhmer MR, Chlon CH, Raju BI, Chin CT, Shevchenko T, Klibanov AL. Focused ultrasound and microbubbles for enhanced extravasation. J Control Release 2010;148:18–24.

Borovjagin AV, Krendelchtchikov A, Ramesh N, Yu DC, Douglas JT, Curiel DT. Complex mosaicism is a novel approach to infectivity enhancement of adenovirus type 5-based vectors. Cancer Gene Ther 2005;12:475–486.

Calliada F, Campani R, Bottinelli O, Bozzini A, Sommaruga MG. Ultrasound contrast agents: Basic principles. Eur J Radiol 1998;27(Suppl 2):S157–S160.

Casey G, Cashman JP, Morrissey D, Whelan MC, Larkin JO, Soden DM, Tangney M, O'Sullivan GC. Sonoporation mediated immunogene therapy of solid tumors. Ultrasound Med Biol 2010;36:430–440.

Caskey CF, Qin S, Dayton PA, Ferrara KW. Microbubble tunneling in gel phantoms. J Acoust Soc Am 2009;125:EL183–EL189.

Chen S, Ding JH, Bekeredjian R, Yang BZ, Shohet RV, Johnston SA, Hohmeier HE, Newgard CB, Grayburn PA. Efficient gene delivery to pancreatic islets with ultrasonic microbubble destruction technology. Proc Natl Acad Sci USA 2006;103:8469–8474.

Chin CT, Raju BJ, Shevchenko T, Klibanov AL. Control and reversal of tumor growth by ultrasound activated microbubbles. In: Proceedings, 2009 IEEE Ultrasonics Symposium, Rome, 20–23 September 2009:77–80.

Choi JW, Kang E, Kwon OJ, Yun TJ, Park HK, Kim PH, Kim SW, Kim JH, Yun CO. Local sustained delivery of oncolytic adenovirus with injectable alginate gel for cancer virotherapy. Gene Ther 2013 March 21; http://dx.doi.org/10.1038/gt.2013.10 [Epub ahead of print].

Choi JW, Lee JS, Kim SW, Yun CO. Evolution of oncolytic adenovirus for cancer treatment. Adv Drug Deliv Rev 2012;64:720–729.

Cosgrove D. Ultrasound contrast agents: An overview. Eur J Radiol 2006;60:324–330.

De Vrij J, Willemsen RA, Lindholm L, Hoeben RC, Bangma CH, Barber C, Behr JP, Briggs S, Carlisle R, Cheng WS,

Dautzenberg IJ, de Ridder C, Dzojic H, Erbacher P, Essand M, Fisher K, Frazier A, Georgopoulos LJ, Jennings I, Kochanek S, Koppers-Lalic D, Kraaij R, Kreppel F, Magnusson M, Maitland N, Neuberg P, Nugent R, Ogris M, Remy JS, Scaife M, Schenk-Braat E, Schooten E, Seymour L, Slade M, Szyjanowicz P, Totterman T, Uil TG, Ulbrich K, van der Weel L, van Weerden W, Wagner E, Zuber G, for the GIANT Consortium. Adenovirus-derived vectors for prostate cancer gene therapy. Hum Gene Ther 2010;21: 795–805.

Department of Defense. UoI. Phase II Study of adenovirus/PSA vaccine in men with hormone-refractory prostate cancer (APP22). Bethesda, MD: National Library of Medicine. Retrieved 2013. Available from, http://clinicaltrials.gov/show/NCT00583024; 2007. NLM Identifier: NCT00583024.

Dijkmans PA, Juffermans LJ, Musters RJ, van Wamel A, ten Cate FJ, van Gilst W, Visser CA, de Jong N, Kamp O. Microbubbles and ultrasound: From diagnosis to therapy. Eur J Echocardiogr 2004;5: 245–256.

Ferrara K, Pollard R, Borden M. Ultrasound microbubble contrast agents: Fundamentals and application to gene and drug delivery. Annu Rev Biomed Eng 2007;9:415–447.

Frenkel V. Ultrasound mediated delivery of drugs and genes to solid tumors. Adv Drug Deliv Rev 2008;60:1193–1208.

Fukazawa T, Matsuoka J, Yamatsuji T, Maeda Y, Durbin ML, Naomoto Y. Adenovirus-mediated cancer gene therapy and virotherapy [review]. Int J Mol Med 2010;25:3–10.

Greber UF, Willetts M, Webster P, Helenius A. Stepwise dismantling of adenovirus 2 during entry into cells. Cell 1993;75:477–486.

Heath CH, Sorace A, Knowles J, Rosenthal E, Hoyt K. Microbubble therapy enhances anti-tumor properties of cisplatin and cetuximab in vitro and in vivo. Otolaryngol Head Neck Surg 2012;146: 938–945.

Howard CM, Forsberg F, Minimo C, Liu JB, Merton DA, Claudio PP. Ultrasound guided site specific gene delivery system using adeno-viral vectors and commercial ultrasound contrast agents. J Cell Physiol 2006;209:413–421.

Kaplan JM. Adenovirus-based cancer gene therapy. Curr Gene Ther 2005;5:595–605.

Kim KH, Dmitriev I, O'Malley JP, Wang M, Saddekni S, You Z, Preuss MA, Harris RD, Aurigemma R, Siegal GP, Zinn KR, Curiel DT, Alvarez RD. A phase I clinical trial of Ad5.SSTR/ TK.RGD, a novel infectivity-enhanced bicistronic adenovirus, in patients with recurrent gynecologic cancer. Clin Cancer Res 2012; 18:3440–3451.

Klibanov AL. Microbubble contrast agents: targeted ultrasound imaging and ultrasound-assisted drug-delivery applications. Invest Radiol 2006;41:354–362.

Koike H, Tomita N, Azuma H, Taniyama Y, Yamasaki K, Kunugiza Y, Tachibana K, Ogihara T, Morishita R. An efficient gene transfer method mediated by ultrasound and microbubbles into the kidney. J Gene Med 2005;7:108–116.

Lindner JR. Microbubbles in medical imaging: Current applications and future directions. Nat Rev Drug Discov 2004;3:527–532.

Lupold SE, Rodriguez R. Adenoviral gene therapy, radiation, and prostate cancer. Rev Urol 2005;7:193–202.

McDannold N, Arvanitis CD, Vykhodtseva N, Livingstone MS. Temporary disruption of the blood-brain barrier by use of ultrasound and microbubbles: Safety and efficacy evaluation in rhesus macaques. Cancer Res 2012;72:3652–3663.

Miller DL, Quddus J. Diagnostic ultrasound activation of contrast agent gas bodies induces capillary rupture in mice. Proc Natl Acad Sci USA 2000;97:10179–10184.

Nie F, Xu HX, Lu MD, Wang Y, Tang Q. Anti-angiogenic gene therapy for hepatocellular carcinoma mediated by microbubble-enhanced ultrasound exposure: An in vivo experimental study. J Drug Target 2008;16:389–395.

Patel P, Wood BJ, Frenkel V, Nguyen D. Enhancement of AdVgTRAIL Gene Therapy using pulsed-high intensity focused ultrasound (HIFU) in a human esophageal carcinoma model in mice. In: Proceedings, Radiological Society of North America meeting, Chicago, 2007.

Price RJ, Skyba DM, Kaul S, Skalak TC. Delivery of colloidal particles and red blood cells to tissue through microvessel ruptures created by targeted microbubble destruction with ultrasound. Circulation 1998; 98:1264–1267.

Shimamura M, Sato N, Taniyama Y, Kurinami H, Tanaka H, Takami T, Ogihara T, Tohyama M, Kaneda Y, Morishita R. Gene transfer into adult rat spinal cord using naked plasmid DNA and ultrasound microbubbles. J Gene Med 2005;7:1468–1474.

Shohet RV, Chen S, Zhou YT, Wang Z, Meidell RS, Unger RH, Grayburn PA. Echocardiographic destruction of albumin microbubbles directs gene delivery to the myocardium. Circulation 2000;101: 2554–2556.

Sirsi SR, Borden MA. Advances in ultrasound mediated gene therapy using microbubble contrast agents. Theranostics 2012;2:1208–1222.

Sirsi SR, Hernandez SL, Zielinski L, Blomback H, Koubaa A, Synder M, Homma S, Kandel JJ, Yamashiro DJ, Borden MA. Poly-plex-microbubble hybrids for ultrasound-guided plasmid DNA delivery to solid tumors. J Control Release 2012;157:224–234.

Song J, Chappell JC, Qi M, VanGieson EJ, Kaul S, Price RJ. Influence of injection site, microvascular pressure and ultrasound variables on microbubble-mediated delivery of microspheres to muscle. J Am Coll Cardiol 2002;39:726–731.

Sorace AG, Saini R, Mahoney M, Hoyt K. Microbubble-mediated ultrasound therapy uptake effects in cell suspensions and cell mono-layers. J Ultrasound Med 2012a;31:S96.

Sorace AG, Saini R, Rosenthal E, Warram JM, Zinn KR, Hoyt K. Optical fluorescent imaging to monitor temporal effects of microbubble-mediated ultrasound therapy. IEEE Trans Ultrason Ferroelectr Freq Control 2013;60:281–289.

Sorace AG, Warram JM, Umphrey H, Hoyt K. Microbubble-mediated ultrasonic techniques for improved chemotherapeutic delivery in cancer. J Drug Target 2012b;20:43–54.

Stieger SM, Caskey CF, Adamson RH, Qin S, Curry FR, Wisner ER, Ferrara KW. Enhancement of vascular permeability with low-frequency contrast-enhanced ultrasound in the chorioallantoic membrane model. Radiology 2007;243:112–121.

Tamosiūnas M, Jurkonis R, Mir LM, Lukosevicius A, Venslauskas MS, Satkauskas S. Adjustment of ultrasound exposure duration to micro-bubble sonodestruction kinetics for optimal cell sonoporation in vitro. Technol Cancer Res Treat 2012;11:375–387.

Treat LH, McDannold N, Zhang Y, Vykhodtseva N, Hynynen K. Improved anti-tumor effect of liposomal doxorubicin after targeted blood-brain barrier disruption by MRI-guided focused ultrasound in rat glioma. Ultrasound Med Biol 2012;38:1716–1725.

Tsunoda S, Mazda O, Oda Y, Iida Y, Akabame S, Kishida T, Shin-Ya M, Asada H, Gojo S, Imanishi J, Matsubara H, Yoshikawa T. Sonopora-tion using microbubble BR14 promotes pDNA/siRNA transduction to murine heart. Biochem Biophys Res Commun 2005;336: 118–127.

Wang JF, Wu CJ, Zhang CM, Qiu QY, Zheng M. Ultrasound-mediated microbubble destruction facilitates gene transfection in rat C6 glioma cells. Mol Biol Rep 2009;36:1263–1267.

Wang X, Liang HD, Dong B, Lu QL, Blomley MJ. Gene transfer with microbubble ultrasound and plasmid DNA into skeletal muscle of mice: Comparison between commercially available microbubble contrast agents. Radiology 2005;237:224–229.

Warram JM, Sorace AG, Saini R, Borovjagin AV, Hoyt K, Zinn KR. Systemic delivery of a breast cancer-detecting adenovirus using targeted microbubbles. Cancer Gene Ther 2012;19:545–552.

Yun CO. Adenovirus-mediated shRNA delivery to cancer. In: Cheng K, Mahato RI, (eds). Advanced delivery and therapeutic applications of RNAi. New York: Wiley; 2013. p. 309–326.

Zhang Q, Wang Z, Ran H, Fu X, Li X, Zheng Y, Peng M, Chen M, Schutt CE. Enhanced gene delivery into skeletal muscles with ultrasound and microbubble techniques. Acad Radiol 2006;13:363–367.

ORIGINAL ARTICLE

Biodistribution of P-selectin targeted microbubbles

Jason M. Warram[1]*, Anna G. Sorace[2]*, Marshall Mahoney[2], Sharon Samuel[1], Bryant Harbin[2], Madhura Joshi[2], Amber Martin[1], Lee Whitworth[1], Kenneth Hoyt[1,2], and Kurt R. Zinn[1,2]

[1]Department of Radiology and [2]Department of Biomedical Engineering, University of Alabama at Birmingham, Birmingham, AL, USA

Abstract

Purpose: To evaluate binding of P-selectin targeted microbubbles (MB) in tumor vasculature; a whole-body imaging and biodistribution study was performed in a tumor bearing mouse model.
Methods: Antibodies were radiolabeled with Tc-99 m using the HYNIC method. Tc-99 m labeled anti-P-selectin antibodies were avidin-bound to lipid-shelled, perfluorocarbon gas-filled MB and intravenously injected into mice bearing MDA-MB-231 breast tumors. Whole-body biodistribution was performed at 5 min ($n = 12$) and 60 min ($n = 4$) using a gamma counter. Tc-99 m-labeled IgG bound IgG-control-MB group ($n = 12$ at 5 min; $n = 4$ at 60 min), Tc-99 m-labeled IgG-control-Ab group ($n = 5$ at 5 min; $n = 3$ at 60 min) and Tc-99 m-labeled anti P-selectin-Ab group ($n = 5$ at 5 min; $n = 3$ at 60 min) were also evaluated. Planar gamma camera imaging was also performed at each time point.
Results: Targeted-MB retention in tumor (60 min: $1.8 \pm 0.3\%$ ID/g) was significantly greater ($p = 0.01$) than targeted-MB levels in adjacent skeletal muscle at both time points (5 min: $0.7 \pm 0.2\%$ ID/g; 60 min: $0.2 \pm 0.1\%$ ID/g) while there was no significant difference ($p = 0.17$) between muscle and tumor retention for the IgG-control-MB group at 5 min.
Conclusions: P-selectin targeted MBs were significantly higher in tumor tissue, as compared with adjacent skeletal tissue or tumor retention of IgG-control-MB.

Introduction

Improving targeted delivery of anti-cancer drugs to a solid primary tumor can improve overall effectiveness of current systemic and targeted therapies, while reducing total dose and systemic toxicity. Ultrasound contrast agents are perfluorocarbon, gas-filled, lipid microbubbles (MBs) with a diameter of 1–3 μm. The stability of MBs within microvasculature, combined with their non-toxic and non-immunogenic properties has led to pre-clinical investigations of MBs to improve tumor delivery of therapeutic compounds [1], plasmids [2] and viral vectors [3]. Various drug delivery strategies have been investigated using MBs to improve cancer therapy. Some pre-clinical research utilizing MB-assisted delivery involves a physical association between the MB and therapeutic compound [2,4]. One such approach includes labeling hydrophilic pDNA to the exterior of protein-shelled MBs using non-covalent interactions [5]. Other studies have taken advantage of the unique lipid shell component in conjunction with lipophilic compounds, such as Paclitaxel, to physically join the compound to the MB core [1,6,7]. Additional approaches involve double-emulsified MBs that physically encapsulate

hydrophilic macromolecules such as pDNA [8], Doxorubicin [9] and adenovirus [10]. In the latter studies, complete encapsulation of the agent was proven advantageous for systemic or localized delivery because the payload was shielded from immune response and sequestering mechanisms. In all of these strategies, the performance of the MB to transport and deliver a molecule to the targeted region is dependent upon the ability of the MB to specifically accumulate within that tissue.

Targeting MBs to commonly over-expressed receptors in a specified region-of-interest have been shown to improve overall MB accumulation at target sites [11,12]. The active targeting of MBs is achieved by conjugating receptor-specific ligands to the outer shell via biotin–avidin chemistry or covalent linkage [13]. Ligand-modified MBs bind specifically to molecular receptors within the vasculature of the targeted tissue, while unbound MBs are filtered from the circulation [14]. Improved MB accumulation using targeted strategies has been demonstrated in the molecular imaging of tumor angiogenesis [15–17], inflammation [13,18,19] and intravascular thrombi [6,7,20]. Radiolabeling MBs is not a novel concept, as many groups are exploring these techniques for dual-modality US/SPECT or US/PET imaging [21–23], as well as assessing MB distribution [24]. Using these established tools, it is hypothesized that we can better evaluate full body evaluation of P-selectin targeted MBs for imaging and drug delivery. One cellular target currently under investigation is the cell adhesion molecule, P-selectin (CD-62 P),

---

*These authors contributed equally to this study.

Address for correspondence: Kurt R. Zinn, Departments of Radiology and Biomedical Engineering, University of Alabama at Birmingham, Birmingham, AL 35294, USA. Tel: +1-205-975-6405. Fax: +1-205-975-6522. E-mail: kurtzinn@uab.edu

RIGHTSLINK()

which is commonly over-expressed in tumor endothelial cells [25]. P-selectin is expressed on stimulated endothelial cells and activated platelets; it contributes to the recruitment of leukocytes in areas of inflammation common in tumor vasculature [26,27]. In addition, the presence of P-selectin permits the adhesion of platelets and cancer cells to the tumor endothelium. Strategies for improving MB accumulation have utilized the expression of P-selectin in echocardiography, atherosclerotic plaque detection, and tumor detection [28–30]. The overexpression of P-selectin in the tumor vasculature by stimulated endothelial cells makes it a viable target for improving intravascular MB retention. In comparison to other targeting options for drug delivery, such as VEGFR2 and $\alpha V \beta 3$ integrin, our group has previously demonstrated that P-selectin showed the highest binding efficiency in SVR mouse endothelial cells, which is the basis for it being chosen in this study for further exploration [30].

The challenges associated with systemically delivered therapeutic agents include both non-specific sequestration and immunogenicity from toxic chemical compounds and viral therapy. The well characterized safety of MBs [31], combined with the ability to target specific molecules within the tumor makes this approach a viable tool for the safe and specific delivery of these agents to improve overall patient treatment and survival. The current study propels this drug delivery technique forward by elucidating the whole-body biodistribution of P-selectin targeted MBs.

Materials and methods

Culture methods and tumor model

MDA-MB-231 breast cancer cell lines were purchased from the American Tissue Type Collection (Manassas, VA) and maintained in DMEM, 10% FBS and 1% L-glutamine. The cell line was cultured at $37\,^{\circ}C$ and 5% CO_2 while maintained to 70–90% confluence before passaging. To generate the tumor model, 2×10^6 cells were subcutaneously implanted in the flank of 6-week-old athymic female nude mice (Frederick Cancer Research, Hartford, CT). Cell numbers were determined with hemocytometer and trypan blue dye exclusion. Tumors were allowed to grow to a mean diameter range of 8–10 mm. Institutional Animal Care and Use Committee (IACUC) at the University of Alabama at Birmingham approved all animal protocols.

Preparation of radiolabeled antibodies

Radiolabeling of biotinylated rat IgG anti mouse CD-62 P (PSGL-1; 553743, BD Pharmingen, San Diego, CA) and biotinylated rat IgG antibody (SouthernBiotech, Birmingham, AL) was performed using the HYNIC method as previously described [32]. Briefly, a fresh 1.8 mmol/L solution of succinimidyl 6-hydrazinonicotinate (HYNIC) in dimethylformamide was prepared. Forty picomoles were transferred to glass vials, followed by freezing at $-90\,^{\circ}C$, and then solutions were vacuum dried using an Advantage Benchtop Freeze Dryer (Virtis Co., Inc., Gardiner, NY) with the shelf temperature at $-75\,^{\circ}C$ and trap at $-90\,^{\circ}C$. The vials were sealed under vacuum and kept frozen at $-80\,^{\circ}C$ until use. Each vial was reconstituted with 1.0 mL of sodium phosphate

buffer (0.15 mol/L, pH 7.8) containing 0.3 mg of IgG antibody (HYNIC/antibody molar ratio of 18) [33]. After 3 h incubation at room temperature, the mixture was transferred to a Slide-A-Lyzer dialysis cassette having 10 000 molecular weight cutoff (Pierce, Rockford, IL) and immersed in 1.0 L phosphate buffered saline (PBS, pH 7.4) overnight at $4\,^{\circ}C$. The HYNIC-modified antibody was labeled with Tc-99 m using $SnCl_2$/tricine as the transfer ligand [34], and unbound Tc-99 m was removed by G-25 Sephadex size-exclusion chromatography. Protein concentrations of the collected fractions were measured by Lowry assay [35]. The level of free Tc-99 m was measured by thin layer chromatography (TLC) using separate strips eluted with saturated saline and methyl ethyl ketone. Experiments were separated into 2 days.

Targeted microbubbles

Streptavidin coated MBs (Targestar-SA) were obtained from Targeson (San Diego, CA). MBs were conjugated to the antibodies by means of biotin–streptavidin chemistry as previously described [30]. Briefly, streptavidin-bound MBs were incubated with the respective antibodies (100 μg per group) for 20 min followed by two times centrifuge washing ($400 \times$ for 3 min) to wash out unbound particles. The amount of antibody used during conjugation served to saturate the available streptavidin on the MB. MB concentration was determined *via* hemocytometer to ensure equal amounts of MBs were injected between groups.

The amount of antibody within the MB dose administered per injection was calculated by dividing activity injected by the decay-corrected specific activity (μCi/μg). To determine the μg/MB, the amount of antibody injected was divided by the number of MB administered per injection. This value was converted to micromoles, and then multiplied by 6.023×10^{17} (molecules per micromole) to yield number of molecules per MB.

Whole-body biodistribution

Prior to experiments, mice were sorted based on tumor sizes to achieve equal distribution of tumor size in all groups. Experiments were performed over a 2-day period with day one biodistribution performed 5 min post-intravenous (tail vein) injection of P-selectin-MB ($n = 12$; 0.274 μg, 2.88×10^5 MB), IgG-control-MB ($n = 12$; 0.363 μg, 2.88×10^5 MB), P-selectin-Ab ($n = 5$; 0.274 μg) and IgG-control-Ab ($n = 5$; 0.363 μg). Day two biodistribution was performed 60 min post-intravenous (tail vein) injection of P-selectin-MB ($n = 4$; 0.239 μg, 2.49×10^5 MB), IgG-control-MB ($n = 4$; 0.378 μg, 2.88×10^5 MB), P-selectin-Ab ($n = 3$; 0.239 μg) and IgG-control-Ab ($n = 3$; 0.378 μg). All injections for MBs and antibody alone were diluted to a total volume of 60 μl with saline. Planar gamma camera imaging was performed on day 2. The biodistribution procedure was performed as previously described [36]. Briefly, syringes containing dose were counted before and after injection using an Atomlab 100-dose calibrator (Biodex Medical Systems, Shirley, NY) to determine the exact dose. At 5 min and 60 min post-dose, animals were sacrificed and all tissues collected in previously weighed scintillation vials. All tissue samples were then weighed and the Tc-99 m activity was measured using a

RIGHTS LINK()

calibrated gamma ray counter (MINAXIg Auto-gamma 5000 series Gamma Counter; Packard Instrument Company), decay corrected to dosing time, and converted to absolute radio-activity. The percentage of injected dose per gram of tissue (%ID/g) was determined and used for comparison.

Gamma camera imaging

Imaging studies were conducted using X-SPECT, a SPECT/CT dual-modality imaging instrument manufactured by Gamma Medica, Inc. (Northridge, CA). Acquisitions (60 s) were performed in planar mode using high-resolution low-energy parallel-hole collimators. Imaging was performed during day two at 4 min and 59 min post-injection. Injection of radioactivity and subsequent imaging was staggered between the groups to account to radionuclide and MB decay. Quantitative analysis was performed using exported images and ImageJ software. ROI masks were generated and applied to each tumor to uniformly measure mean pixel intensity. Data shown as mean pixel intensity $\pm$ SD.

Statistical analysis

Statistical analysis was completed using the SAS 9.2 software (Cary, NC). Analysis of variance (ANOVA) was used to analyze the differences between the group means and variation among and within the groups. Comparisons were performed using a Tukey–Kramer method (Tukey's HSD) multiple comparisons test. When comparing % ID/g per tissue within the same animal (e.g. muscle versus tumor), a paired t-test was utilized. All data is given as mean $\pm$ standard deviation (SD). A difference of $p < 0.05$ was considered statistically significant.

Results

Radiolabeling

The antibodies and MBs were successfully labeled with Tc-99 m, with 4% or less free Tc-99 m in the preparations. For day one radiolabeling, specific activity was determined to be 37.25 µCi/µg for the anti P-selectin radiolabeled antibody and 33.61 µCi/µg for the rat IgG radiolabeled antibody. During day 2 radiolabeling, specific activity was determined to be 22.04 µCi/µg for the anti P-selectin radiolabeled antibody and 29.54 µCi/µg for the rat IgG radiolabeled antibody. Values for µg/MB and antibody molecules/MB are presented in Table 1.

P-selectin-MB retention in liver, spleen and lungs

Liver retention was significantly higher ($p < 0.05$) for the IgG-control-MB group (48.5 $\pm$ 7.3% ID/g at 5 min,

Table 1. µg/MB and antibody molecules/MB for P-selectin-MB and IgG-control-MB.

	P-selectin-MB (day 1)	P-selectin-MB (day 2)	IgG-control-MB (day 1)	IgG-control-MB (day 2)
µg/MB	9.55×10^{-7}	8.33×10^{-7}	1.26×10^{-6}	1.32×10^{-6}
Antibody molecules/MB	3.83×10^{6}	3.34×10^{6}	5.07×10^{6}	5.28×10^{6}

42.7 $\pm$ 2.1% ID/g at 60 min) compared to all other groups (Figure 1a). Liver retention in all groups remained stable from 5 to 60 min with the exception of the P-selectin-Ab which decreased significantly ($p < 0.05$) from 15.7 $\pm$ 1.8% ID/g at 5 min to 9.2 $\pm$ 3.1% ID/g at 60 min. Notably, liver retention was 82 and 84% higher at both 5 and 60 min in the IgG-control-MB group compared to the P-selectin-MB group. For the spleen, retention levels were greater for the MB groups compared with Ab groups, with no significant difference ($p > 0.05$) between P-selectin-MB (16.9 $\pm$ 6.4% ID/g at 5 min, 23.4 $\pm$ 6.5% ID/g at 60 min) and IgG-control-MB (20.6 $\pm$ 7.4% ID/g at 5 min, 18.0 $\pm$ 6.6% ID/g at 60 min) at the 5 and 60 min time points (Figure 1b). Lung retention remained highest in the MB groups at both time points, however IgG-control-MB was significantly higher ($p < 0.05$) than P-selectin-MB at both 5 min (100.2 $\pm$ 19.3% ID/g for IgG-control-MB, 56.3 $\pm$ 10.1% ID/g for P-selectin-MB) and 60 min (61.7 $\pm$ 4.1% ID/g for IgG-control-MB, 42.4 $\pm$ 4.1% ID/g for P-selectin-MB; Figure 1c).

P-selectin-MB clearance in blood and kidney

Blood clearance from 5 min (26.4 $\pm$ 4.4% ID/g) to 60 min (3.6 $\pm$ 0.5% ID/g) was greatest ($p < 0.01$) for the P-selectin-MB group (87%), while the IgG-control-MB group (9.9 $\pm$ 0.9% ID/g at 5 min, 9.4 $\pm$ 1.2% ID/g at 60 min) was not significantly different ($p > 0.05$; Figure 2a). Likewise, the blood clearance was significantly greater ($p < 0.05$) for the P-selectin-Ab (79%) over the control antibody (42%) from 5 min to 60 min. For the kidneys, there was significantly greater ($p < 0.05$) retention of the P-selectin-MB (12.9 $\pm$ 1.4% ID/g) over IgG-control-MB (8.8 $\pm$ 2.3% ID/g) at the 5 min time point. However, P-selectin-MB were significantly cleared ($p < 0.05$) at the 60 min time point (9.1 $\pm$ 0.6% ID/g), while the IgG-control-MB retention was not significantly different at the 60 min time point (10.2 $\pm$ 2.3% ID/g; Figure 2b).

P-selectin-MB retention in other tissues

Figure 3 shows the retention of P-selectin-MB at the 5 and 60 min time points in heart, stomach, large intestine, small intestine, cecum, reproductive organs, brain and femur. The greatest P-selectin-MB retention was observed in the stomach (12.2 $\pm$ 0.9% ID/g) at 60 min. The stomach also demonstrated the greatest increase in retention from 5 min to 60 min (3.2 $\pm$ 1.4% ID/g at 5 min). The cecum also demonstrated an increase in P-selectin-MB retention from 5 min (12.2 $\pm$ 0.8% ID/g) to 60 min (12.2 $\pm$ 0.8% ID/g). The heart (6.8 $\pm$ 1.6% ID/g at 5 min, 1.77 $\pm$ 0.1% ID/g at 60 min) and brain (0.7 $\pm$ 0.2% ID/g at 5 min, 0.2 $\pm$ 0.03% ID/g at 60 min) showed the only significant decrease ($p < 0.05$) in retention over time. IgG-control-MB exhibited similar trends in these tissues compared to P-selectin-MB ($p > 0.05$).

P-selectin-MB retention in tumor and muscle

For the tumor, there was significantly higher ($p < 0.05$) retention of P-selectin-MB (1.3 $\pm$ 0.4% ID/g) over IgG-control-MB (0.4 $\pm$ 0.1% ID/g) at 5 min (Figure 4). Tumor retention for all groups increased from 5 to 60 min, which was unique to tumor. P-selectin-MB retention in tumor

Figure 1. Comparison of percent injected dose per gram (%ID/g) values at 5 min and 60 min for P-selectin targeted microbubbles (MB), IgG targeted control MB, P-selectin antibody, and IgG control in (a) liver, (b) spleen, and (c) lungs. Data are means ± SD. Asterisk denotes statistically significant difference, $p < 0.05$.

Figure 2. Comparison of percent injected dose per gram (%ID/g) values at 5 min and 60 min for P-selectin targeted microbubbles (MB), IgG targeted control MB, P-selectin antibody, and IgG control in (a) blood and (b) kidney. Data are means ± SD. Asterisk denotes statistically significant difference, $p < 0.05$.
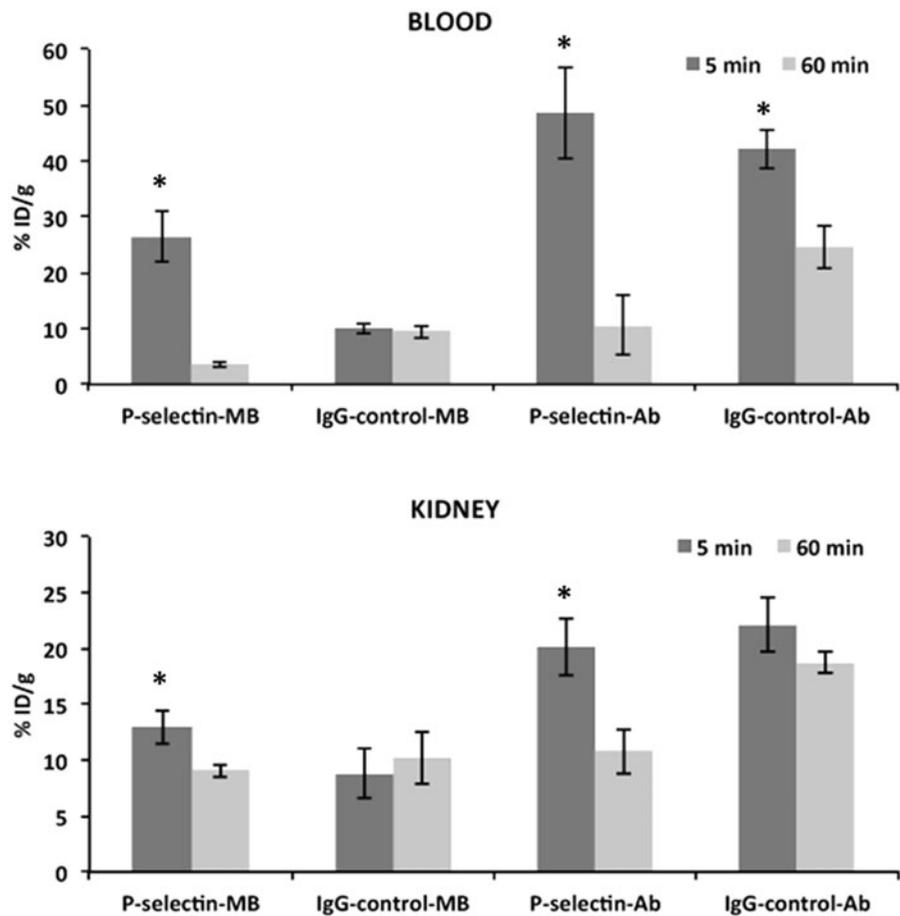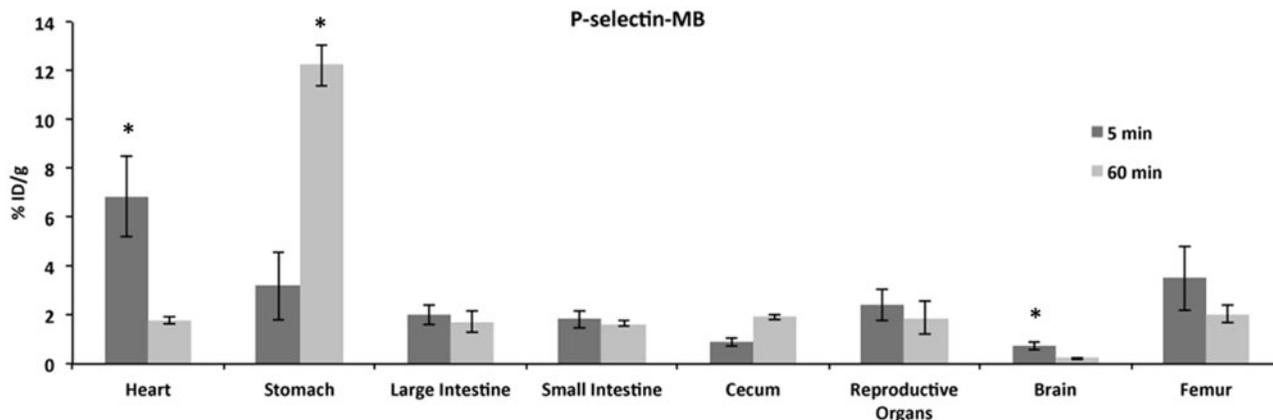
Figure 3. Comparison of percent injected dose per gram (% ID/g) values at 5 min and 60 min for P-selectin targeted microbubbles in heart, stomach, large intestine, small intestine, cecum, reproductive organs, brain and femur. Data are means ± SD. Asterisk denotes statistically significant difference, $p < 0.05$.
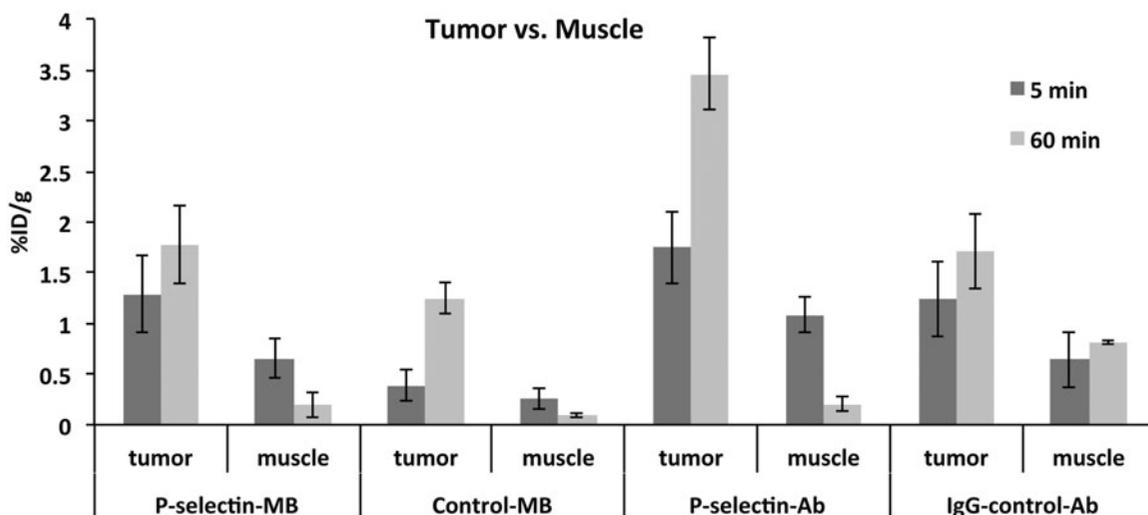
Figure 4. Comparison of percent injected dose per gram (%ID/g) values in tumor and muscle tissue at 5 min and 60 min P-selectin targeted microbubbles (MB), IgG targeted control MB, P-selectin antibody and IgG control groups. Data are means ± SD.

$(1.3 \pm 0.4\%$ ID/g at 5 min, $1.8 \pm 0.4\%$ ID/g at 60 min) was significantly greater ($p < 0.01$) than P-selectin-MB levels in adjacent skeletal muscle at both time points ($0.6 \pm 0.2\%$ ID/g at 5 min, $0.2 \pm 0.1\%$ ID/g at 60 min). There was no significant difference ($p = 0.17$) between muscle ($0.3 \pm 0.1\%$ ID/g) and tumor ($0.4 \pm 0.1\%$ ID/g) retention for the IgG-control-MB group at 5 min. The greatest tumor retention occurred at the 60 min time point with the P-selectin-Ab group ($3.5 \pm 0.3\%$ ID/g).

Planar gamma camera imaging

Planar gamma camera imaging was performed to compare with whole-body biodistribution. Figure 5(a) shows analysis of mean pixel intensity in tumor at 5 and 60 min time points for P-selectin-MB and IgG-control-MB groups. The trend of increased tumor retention for the MB groups was observed in the P-selectin-MB exhibiting a 98% increase ($p = 0.03$) over time ($6.0 \pm 2.23\%$ at 5 min, 11.9 ± 3.93 at 60 min). The IgG-control-MB group showed a 57% increase ($p = 0.07$) from 5 to 60 min ($4.4 \pm 0.4\%$ at 5 min, $6.9 \pm 1.8\%$ at 60 min).

In Figure 5(b), a representative image of planar gamma camera imaging shows Tc-99 m tumor retention for the P-selectin-MB group at 60 min.

Discussion

Accurate measurement of targeted MBs and appropriate controls, in all tissues will aid in the development of these novel-imaging agents. These steps establish specific targeting, as well as non-target tissues involved in elimination. Reported here is the whole body biodistribution of tumor bearing mice after intravenous injection of P-selectin-MBs at 5 and 60 min following systemic injections. Due to the relatively short half-life of MBs, these time points were chosen to best represent initial uptake in individual organs (5 min), as well as retention and clearance in those organs (60 min). This full body biodistribution comparing P-selectin-MBs and control MBs can be more generally applied for other mechanisms to target MBs.

Tumor retention of P-selectin-MBs was greater than IgG-control-MBs with a 3.2-fold enhancement of MB
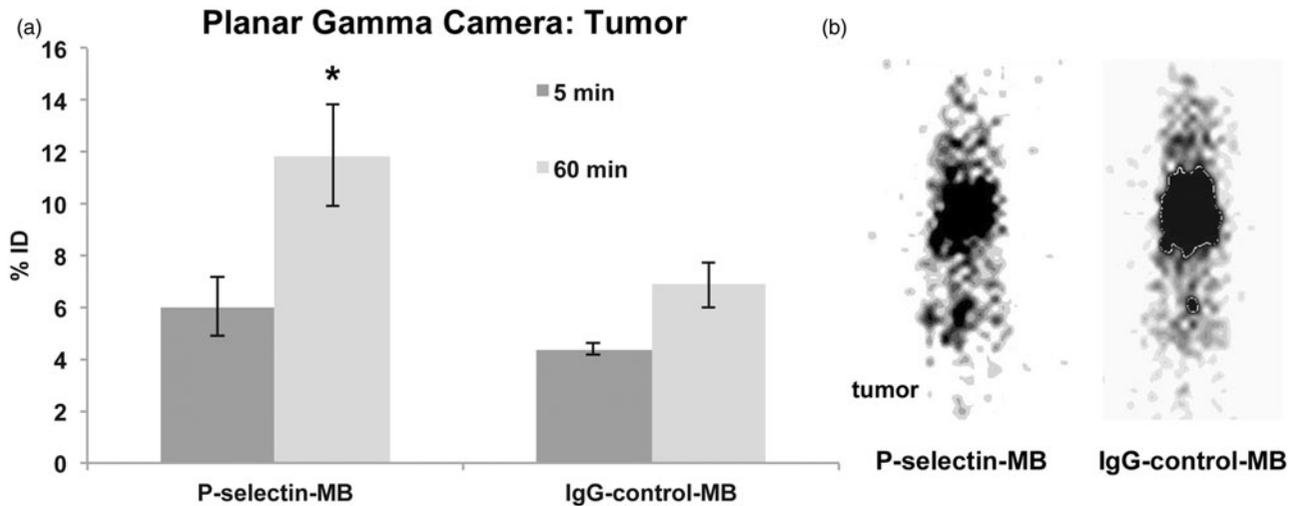
Figure 5. (a) Comparison of percent injected dose (%ID) at 5 min and 60 min during planar gamma camera imaging between P-selectin targeted microbubbles (MB) and IgG targeted control MB in tumor tissue. Data are means ± SD. (b) Representative image of P-selectin targeted MB during planar gamma camera imaging at 60 min. Asterisk denotes statistically significant difference, $p < 0.05$.

accumulation. In addition, there was greater retention of P-selectin-MBs in the tumor compared with adjacent skeletal muscle at both time points, 2-fold at 5 min and 9.3-fold at 60 min. This trend of enhanced tumor accumulation by P-selectin targeting was also observed in the antibody alone groups with greater tumor retention of P-selectin-Ab compared to the IgG-control-Ab. These results confirm the hypothesis that P-selectin targeting is beneficial for MB delivery to tumor. An observed trend that was unique to the tumor tissue was the increase in retention from 5 min to 60 min for all groups. This could be attributed to the enhanced permeability and retention (EPR) effect common to tumor tissue [37]. At 60 min post-injection, it is hypothesized that all the MBs have disintegrated and released their targeted antibodies or have been excreted due to their estimated 2-min half-life. Therefore, the EPR effect is generally suggesting entrapment of the targeted antibodies within the tumor, which can be especially beneficial for tumor drug delivery [38]. Differences in this EPR effect within the tumor as known to vary by tumor vascularity, tumor type, as well as size and properties of the molecule delivered. In a study by Willmann et al. [24], F-18 labeled anti-VEGFR2 MBs were evaluated in angiosarcoma tumor bearing mice using dynamic micro-PET imaging [24]. In that study, tumor retention was reported to be 1.14%ID/g at 4 min post-iv injection and 1.35%ID/g at 60 min post-iv injection while skeletal muscle retention was reported unchanged at 0.84% ID/g at 4 and 60 min. These results were relatively similar to the current study findings, however the deviation between the tumor and muscle tissue was greater for the P-selectin-MBs, which could also be attributed to the different modality, tumor type and receptor density used within the studies.

For the filtration organs, Tc-99 m liver accumulation remained stable from 5 to 60 min for all groups except the P-selectin-Ab group, which was significantly reduced by 41%. This observation of static retention in the liver was also observed in the previously mentioned study performed by Willmann et al. These findings would imply that the capacity of the liver to sequester and process the injected doses

requires more than 60 min. Delayed liver clearance was also shown to occur in a similar study of un-targeted MB biodistribution where MB clearance in the liver was first observed at the 6 h time point [39]. This retention by the liver is most likely due to MB uptake by Kupffer cells, whose normal function is to phagocytose foreign particles, and have been shown to play a crucial role in MB uptake in the liver [3]. At each time point, the lung and liver retention was significantly higher for the IgG-control-MB group compared to the P-selectin-MB group. However, P-selectin-MB retention was greater than IgG-control-MB group in the blood and tumor at each time point, which would account for the lack of retention in liver and lung. Unique to the lung, Tc-99 m retention was significantly greater in the MB groups at both time points compared to antibody alone. Considering the minor amount of pulmonary macrophage contribution to lung clearance in mice [40], the increased MB retention could be explained by the non-specific pulmonary entrapment that often occurs using MBs with a diameter greater than 5 μm [41]. In the spleen, there was a slightly higher retention of MB groups compared with antibody alone; this was most likely caused by previously reported involvement of splenic macrophages and mononuclear phagocyte system in the clearance of MBs [2]. There was no significant difference in the spleen for the MB groups at 5 and 60 min however there was a significant decrease in targeted and control antibody from 5 to 60 min, a trend that further supported the role of splenic macrophages to engulf MBs in the spleen. In the kidneys, there was greater retention of the radiolabeled antibody groups compared to the MB groups at 5 min, a trend that was also observed in the Willmann et al. [24] study. However, there was a significant clearance of both P-selectin-MB and P-selectin-Ab in the kidneys that was not observed in the IgG control groups suggesting an additional benefit of targeting to improve P-selectin-MB circulation and bioavailability while limiting kidney accumulation over time. Expediting kidney clearance could prove useful in decreasing systemic circulation of unbound particles. As expected, organs filtered MBs and antibodies differently, illustrating the importance of the

control groups used during the whole-body biodistribution. This analysis also demonstrates the differences between targeted and control MBs, with decreased filtration of targeted MBs compared to controls.

When analyzing P-selectin-MBs alone, retention was highest at the 5 min time point in the lung (56.3% ID/g) followed by the blood (26.4% ID/g) and then the liver (26.1% ID/g). The relatively high signal in the stomach and cecum is attributed to the normal gut localization of free Tc-99 m pertechnetate that ultimately is an artifact of the radiolabeling strategy used in this study [42]. At the 60-min time point, P-selectin-MB retention remained relatively constant in the lung, liver, and spleen however there was an 86% clearance in the blood. This represented the greatest amount of blood clearance observed in all groups from 5 to 60 min. The constant levels in lung, liver and spleen suggest the Tc-99 m-labeled P-selectin was not released from the MBs in those tissues. Similarly, the blood clearance suggests the Tc-99 m-labeled P-selectin remained with the MBs and was also not released into the circulation where a longer half-life would be expected.

While P-selectin is overexpressed in tumor vasculature, it is also expressed in other regions of the body, including inflammation processes. This could be a limitation to the study; however, it was shown that targeting does enhance the retention of the targeted groups in the tumor when compared to controls. Other targeted agents explored in cancer therapies including VEGFR2, ICAM-1 and integrin $\alpha_V\beta_3$ are also expressed in other tissues, and not specific to the tumor. Further studies would be beneficial to compare the performance of P-selectin targeted MBs to alternate targeted MBs. Also, there was significant amount of blood clearance after injection of the P-selectin-MB group in comparison to the other groups, exhibiting the necessary traits for filtration. Differences in the blood flow and shear stress can directly affect targeting and retention of molecules within a region-of-interest. There has recently been studies examining P-selectin targeting in ischemic tissues where blood flow is altered [43,44], however it has also been shown that targeting and shear stress is not linearly related [45]. The difference in blood flow is a limitation when comparing skeletal muscle to tumor. This study relies on targeting a receptor which is overexpressed within the tumor, and limitations included, still shows increased retention of targeted MBs over control MBs. Differences in blood flow also directly affect Abs and MBs differently, as MBs have a much shorter half-life than Ab. Ab have an estimated 11-day half-life [46], while MBs have an estimated 2-min half-life [2]. These differences can directly affect tumor uptake, as well as organ filtration and sequestration. MB half-life is dependent both on size of the MB and concentration in which they are injected, which can have a direct effect of the stability of the delivery system. The more stable a drug or molecule, the greater chance at heightened efficiency to for delivery to the intended site, leading to improved drug delivery and imaging.

One limitation of this study was the use of avidin chemistry to adhere the antibody to the MB. While this strategy ensures a stable bioconjugate, the avidin utility reduces the translational potential of the targeted MB construct due to the immunogenicity of the avidin molecule.

Alternative strategies of MB targeting being developed include the use of targeted peptides that are covalently bound to MBs. Initial studies using this motif have been performed and results suggest the strategy to be safe and specific [16,47]. One study recently concluded a phase 0 clinical trial using VEGFR2 as the targeting moiety during prostate cancer evaluation [48]. This component would allow for a more feasible clinical translation of targeted MBs for both imaging and drug delivery. This study reveals interesting results for whole body interactions of targeted microbubble drug delivery, which has potential to lead to future investigations regarding individual organ uptake. A limitation to this study is organ information is only available at the 5- and 60-min time point. Utilizing ultrasound, SPECT or PET, future investigations with dynamic imaging of targeted microbubbles could also be evaluated in specific individual organs or tumor for addition information regarding uptake and clearance. Although there are limitations, this study provides initial evidence of a promising tool for targeted drug delivery using P-selectin and ultrasound contrast agents.

Conclusions

If MBs are continued to be investigated as drug delivery carriers, this study demonstrates that targeting improves tumor retention compared to non-targeting. The study also shows that targeting MBs to P-selectin reduces liver and lung retention compared to non-targeted MBs. While there is more MB retention in all tissues compared to tumor tissue, there is less retention of targeted MBs in tissues and greater tumor retention relative to non-targeted MBs. With the potential of targeted MBs to improve CEUS and drug delivery in patients, the current work is invaluable to elucidate the systemic biodistribution of targeted MBs in general. The innate role of P-selectin to sequester platelets and rolling monocytes is well suited to reproduce the desired mechanism for vascular MB adhesion. The P-selectin molecule is a promising candidate to improve MB accumulation in target tissues; however other cell adhesion molecules and receptors should be continually investigated and may prove to be more efficacious. This study provides validation of P-selectin targeted MBs as a more specific approach for systemic drug delivery in a solid tumor.

Declaration of interest

References

1. Tartis MS, McCallan J, Lum AF, et al. Therapeutic effects of paclitaxel-containing ultrasound contrast agents. Ultrasound Med Biol 2006;32:1771–80.
2. Ferrara K, Pollard R, Borden M. Ultrasound microbubble contrast agents: fundamentals and application to gene and drug delivery. Annu Rev Biomed Eng 2007;9:415–47.
3. Taylor SL, Rahim AA, Bush NL, et al. Targeted retroviral gene delivery using ultrasound. J Gene Med 2007;9:77–87.

4. Tinkov S, Bekeredjian R, Winter G, Coester C. Microbubbles as ultrasound triggered drug carriers. J Pharm Sci 2009;98:1935–61.

5. Korpanty G, Chen S, Shohet RV, et al. Targeting of VEGF-mediated angiogenesis to rat myocardium using ultrasonic destruction of microbubbles. Gene Ther 2005;12:1305–12.

6. Unger EC, McCreery TP, Sweitzer RH, et al. Acoustically active liposphere containing paclitaxel: a new therapeutic ultrasound contrast agent. Invest Radiol 1998;33:886–92.

7. Unger EC, McCreery TP, Sweitzer RH, et al. *In vitro* studies of a new thrombus-specific ultrasound contrast agent. Am J Cardiol 1998;81:58–61.

8. Hauff P, Seemann S, Reszka R, et al. Evaluation of gas-filled microparticles and sonoporation as gene delivery system: feasibility study in rodent tumor models. Radiology 2005;236:572–8.

9. Mayer CR, Geis NA, Katus HA, Bekeredjian R. Ultrasound targeted microbubble destruction for drug and gene delivery. Expert Opin Drug Deliv 2008;5:1121–38.

10. Warram JM, Sorace AG, Saini R, et al. Systemic delivery of a breast cancer-detecting adenovirus using targeted microbubbles. Cancer Gene Ther 2012;19:545–52.

11. Klibanov AL. Microbubble contrast agents: targeted ultrasound imaging and ultrasound-assisted drug-delivery applications. Invest Radiol 2006;41:354–62.

12. Klibanov AL, Rychak JJ, Yang WC, et al. Targeted ultrasound contrast agent for molecular imaging of inflammation in high-shear flow. Contrast Media Mol Imaging 2006;1:259–66.

13. Lindner JR. Microbubbles in medical imaging: current applications and future directions. Nat Rev Drug Discov 2004;3:527–32.

14. Klibanov AL. Ligand-carrying gas-filled microbubbles: ultrasound contrast agents for targeted molecular imaging. Bioconjug Chem 2005;16:9–17.

15. Leong-Poi H, Christiansen J, Klibanov AL, et al. Noninvasive assessment of angiogenesis by ultrasound microbubbles targeted to alpha-v integrins. Circulation 2003;107:455–60.

16. Weller GE, Wong MK, Modzelewski RA, et al. Ultrasonic imaging of tumor angiogenesis using contrast microbubbles targeted via the tumor-binding peptide arginine-arginine-leucine. Cancer Res 2005; 65:533–9.

17. Sorace AG, Saini R, Mahoney M, Hoyt K. Molecular ultrasound imaging using a targeted contrast agent for assessing early tumor response to antiangiogenic therapy. J Ultrasound Med 2012;31: 1543–50.

18. Behm CZ, Kaufmann BA, Carr C, et al. Molecular imaging of endothelial vascular cell adhesion molecule-1 expression and inflammatory cell recruitment during vasculogenesis and ischemia-mediated arteriogenesis. Circulation 2008;117:2902–11.

19. Lindner JR. Contrast ultrasound molecular imaging of inflammation in cardiovascular disease. Cardiovasc Res 2009;84:182–9.

20. Kaufmann BA, Lindner JR. Molecular imaging with targeted contrast ultrasound. Curr Opin Biotech 2007;18:11–16.

21. Lazarova N, Causey PW, Foster FS, et al. Ultrasound/SPECT dual-modality imaging platform using 99mTc-labeled microbubbles. Nucl J Nucl Med 2009;50:569.

22. Lazarova N, Causey PW, Lemon JA, et al. The synthesis, magnetic purification and evaluation of 99 m Tc-labeled microbubbles. Nucl Med Biol 2011;38:1111–18.

23. Liao AH, Wu SY, Wang HE, et al. Evaluation of 18 F-targetd perfluorocarbon-filled albumin microbubbles as a probe for microUS and microPET in tumor-bearing mice. Ultrasonics 2013; 2:320–7.

24. Willmann JK, Cheng Z, Davis C, et al. Targeted microbubbles for imaging tumor angiogenesis: assessment of whole-body biodistribution with dynamic micro-PET in mice. Radiology 2008;249: 212–19.

25. Borsig L, Wong R, Feramisco J, et al. Heparin and cancer revisited: mechanistic connections involving platelets, P-selectin, carcinoma mucins, and tumor metastasis. Proc Natl Acad Sci 2001;98:3352–7.

26. Geng JG, Chen M, Chou KC. P-selectin cell adhesion molecule in inflammation, thrombosis, cancer growth and metastasis. Curr Med Chem 2004;11:2153–60.

27. Stone JP, Wagner DD. P-selectin mediates adhesion of platelets to neuroblastoma and small cell lung cancer. J Clin Invest 1993;92: 804–13.

28. Ferrante EA, Pickard JE, Rychak J, et al. Dual targeting improves microbubble contrast agent adhesion to VCAM-1 and P-selectin under flow. J Control Release 2009;140:100–7.

29. Su CH, Chang CY, Wang HH, et al. Ultrasonic microbubble-mediated gene delivery causes phenotypic changes of human aortic endothelial cells. Ultrasound Med Biol 2010;36:449–58.

30. Warram JM, Sorace AG, Saini R, et al. A triple-targeted ultrasound contrast agent provides improved localization to tumor vasculature. J Ultrasound Med 2011;30:921–31.

31. Aggeli C, Felekos I, Siasos G, et al. Ultrasound contrast agents: updated data on safety profile. Curr Pharm Des 2012;18:2253–8.

32. Kim H, Morgan DE, Buchsbaum DJ, et al. Early therapy evaluation of combined anti-death receptor 5 antibody and gemcitabine in orthotopic pancreatic tumor xenografts by diffusion-weighted magnetic resonance imaging. Cancer Res 2008;68:8369–76.

33. Abrams MJ, Juweid M, Tenkate CI, et al. Technetium-99 m-human polyclonal IgG radiolabeled via the hydrazino nicotinamide derivative for imaging focal sites of infection in rats. J Nucl Med 1990;31:2022–8.

34. Larsen SK, Solomon HF, Caldwell G, Abrams MJ. [99mTc]tricine: a useful precursor complex for the radiolabeling of hydrazinoni-cotinate protein conjugates. Bioconjug Chem 1995;6:635–8.

35. Lowry OH, Rosebrough NJ, Farr AL, Randall RJ. Protein measurement with the Folin phenol reagent. J Biol Chem 1951; 193:265–75.

36. Zinn KR, Buchsbaum DJ, Chaudhuri TR, et al. Noninvasive monitoring of gene transfer using a reporter receptor imaged with a high-affinity peptide radiolabeled with 99mTc or 188Re. J Nucl Med 2000;41:887–95.

37. Iyer AK, Khaled G, Fang J, Maeda H. Exploiting the enhanced permeability and retention effect for tumor targeting. Drug Discov Today 2006;11:812–18.

38. Maeda H. Macromolecular therapeutics in cancer treatment: the EPR effect and beyond. J Controlled Release 2012;164:138–44.

39. Perkins AC, Frier M, Hindle AJ, et al. Human biodistribution of an ultrasound contrast agent (Quantison) by radiolabelling and gamma scintigraphy. Br J Radiol 1997;70:603–11.

40. Brain JD, Molina RM, DeCamp MM, Warner AE. Pulmonary intravascular macrophages: their contribution to the mononuclear phagocyte system in 13 species. Am J Physiol 1999;276:L146–54.

41. Lindner JR, Song J, Jayaweera AR, et al. Microvascular rheology of definity microbubbles after intra-arterial and intravenous administration. J Am Soc Echocardiogr 2002;15:396–403.

42. Zuckier LS, Dohan O, Li Y, et al. Kinetics of perrhenate uptake and comparative biodistribution of perrhenate, pertechnetate, and iodide by NaI symporter-expressing tissues *in vivo*. J Nucl Med 2004;45:500–7.

43. Ryu JC, Davidson BP, Xiw A, et al. Molecular imaging of the paracrine proangiogenic effects of progenitor cell therapy in limb ischemia. Mol Cardiol 2013;127:710–19.

44. Carr CL, Qi Y, Davidson B, et al. Dysregulated selectin expression and monocyte recruitment during ischemia-related vascular remodeling in diabetes mellitus. Arterioscler Thromb Vasc Biol 2011;31:2526–33.

45. Takalkar AM, Klibanov AL, Rychak JJ, et al. Binding and detachment dynamics of microbubbles targeted to P-selectin under controlled shear flow. J Control Release 2004;96:473–82.

46. Abulrob A, Brunette E, Slinn J, et al. *In vivo* optical imaging of ischemic blood-brain barrier disruption. Methods Mol Biol 2011; 763:423–39.

47. Anderson CR, Hu X, Zhang H, et al. Ultrasound molecular imaging of tumor angiogenesis with an integrin targeted microbubble contrast agent. Invest Radiol 2011;46:215–24.

48. Pochon S, Tardy I, Bussat P, et al. BR55: a lipopeptide-based VEGFR2-targeted ultrasound contrast agent for molecular imaging of angiogenesis. Invest Radiol 2010;45:89–95.

Four-dimensional Molecular Ultrasound Imaging of Tumor Angiogenesis in a Preclinical Animal Model of Prostate Cancer

Kenneth Hoyt, Marshall Mahoney, Anna G. Sorace
Departments of Radiology and Biomedical Engineering
University of Alabama at Birmingham
Birmingham, AL USA

Abstract—**This article evaluated volumetric molecular ultrasound (US) imaging with multi-targeted microbubble (MB) contrast agents for detection of angiogenic imaging biomarkers in a preclinical cancer model. Imaging was performed using a modified US system (Ultrasonix Medical Corp) equipped with a 4-dimensional (4D) transducer. Image processing software separated the US signal originating from intravascular MBs that were bound to the overexpressed targets from the freely circulating and unattached contrast agent. Molecular US imaging using targeted MBs was compared to results obtained using non-specific control MBs in the same prostate-cancer bearing mouse. Molecular US signals were significantly higher when imaging the targeted MBs versus imaging of control contrast agent ($p < 0.001$). Specifically, it was found that molecular US imaging of the targeted MB contrast agent produced a considerable mean intratumoral enhancement of 19.5 ± 2.2 dB. A significant inverse correlation was found between the molecular US signal and fractional tumor enhancement ($\rho = -0.56$, $p = 0.02$). This suggests that as the spatial distribution of the molecular US signal increases, the average intensity of the intratumoral reporter signal decreases. This finding could identify when the neovascularity is inadequate to meet the metabolic demands of the tumor, creating a strong angiogenic response. This high angiogenic response is typically found in aggressive cancers and during early stages of tumor growth. Therefore, molecular US imaging may improve US for the early detection of cancer and help distinguish indolent from aggressive disease.**

Keywords—angiogenesis; contrast agent; microbubbles; molecular imaging; prostate cancer; ultrasound

I. INTRODUCTION

An early development that differentiates normal from cancerous tissue is the angiogenic process by which the tumor develops its blood supply from pre-existing vessels. The morphology of this neovascularity is often quantified as the intratumoral microvessel density (MVD) and has been shown to be an independent predictor of malignant disease [1, 2]. Angiogenesis is essential for tumor growth beyond a few millimeters in size and plays a major factor in metastatic disease. Neovascularity can form a substantial portion of the mass of malignant tumors [3]. Given that knowledge, medical imaging techniques are being investigated for discriminating malignant from benign disease based on tumor vascularization profiles. Tumor angiogenesis is an important biomarker for disease which can be visualized with cancer imaging techniques. This advances the potential to noninvasively characterize tissues for detection and monitoring of cancer.

Molecular imaging permits noninvasive visualization of molecular and cellular events inside the human body. With the development of red blood cell-sized intravascular microbubble (MB) contrast agents, ultrasound (US) is an emerging and promising molecular imaging modality. Importantly, the surface of these MBs can be coated with ligands whose target receptors are known to be overexpressed in diseased tissue. While unbound circulating MBs are cleared from the bloodstream within minutes, targeted agents attach to specific endothelial markers providing contrast enhancement via localized accumulation. Recent studies have demonstrated the benefit of targeted MBs for molecular US imaging of overexpressed receptors associated with tumor angiogenesis [4-7]. Importantly, changes in receptor expression (*e.g.*, due to disease progression or response to drug intervention) were shown during *in vitro* studies to be positively correlated to targeted MB binding and accumulation [8] and *in vivo* to molecular US imaging-based receptor measurements [9].

Being a relatively new modality, molecular US imaging has predominately been restricted to planar measurements, which inherently limits a comprehensive, spatial study of the entire disease or tumor burden. In fact, it has been suggested that planar studies risk misrepresenting more complex heterogeneous tissues and that volumetric analyses provide a more robust molecular US imaging assessment of disease biomarkers [10]. Our group recently detailed contrast-enhanced US imaging implemented on commercially available technology that acquires volumetric image data for the purpose of vascularity mapping [11, 12] and monitoring early response to drug treatment [13]. Here we introduce a volumetric molecular US imaging technique using the same platform technology and evaluate performance with a preclinical animal model of prostate cancer.

II. METHODOLOGY

A. Contrast agent preparation

Streptavidin-coated MB contrast agent (Targestar-SA, San Diego, CA) was conjugated with biotinylated rat IgG antibodies

against mouse VEGFR2 (20 μg; 13-5821, eBioscience, San Diego, CA), p-selectin (20 μg; 553743, BD Biosciences, San Jose, CA), and αVβ3-integrin (20 μg; 13-0512, eBioscience). Briefly, streptavidin-bound MBs were incubated with antibody for 20 min, followed by centrifuge washing to remove any unbound particles. For a control group, 60 μg of biotinylated rat IgG antibody (Southern Biotech, Birmingham, AL) was used to generate an isotype targeted contrast agent. All MB concentrations were approximated using a hemocytometer.

B. Cell culture and animal preparation

Human PC3 prostate cancer cells were purchased from the American Type Culture Collection (Manassas, VA). Cells were maintained in Dulbecco's modified Eagle's medium, 10% fetal bovine serum, and 1% L-glutamine. Cells were grown at 37°C in 5% carbon dioxide. Cell numbers were determined with a hemocytometer and trypan blue dye exclusion. Eighteen 6-week-old athymic male nude mice were obtained from the Frederick Cancer Research Center (Frederick, MD). Animals were implanted with 2×10^6 PC3 cells in the left flank. Tumor implants were monitored by caliper measurements and allowed to grow for 6 weeks (average tumor size, 3.06 ± 0.71 cm^2). Animals were randomly divided into two groups.

C. Molecular ultrasound imaging

Either targeted or control MB contrast agent was intravenously injected (4×10^7 MBs per animal in a 0.1 mL dose) in the tail vein. Two min after injection, each animal was imaged for 10 sec using a low-intensity pulse-inversion harmonic imaging mode implemented on the portable SONIX Tablet US system (Ultrasonix Medical Corp, Richmond, BC) equipped with a 4DL14-5/38 transducer (5 MHz transmit and 10 MHz receive). At this initial phase of imaging, US images of the tumor depicted both bound and systemically flowing MB contrast agent. An external unfocused single-element US transducer (2.25 MHz, Olympus Panametrics, Waltham, MA) was positioned at the far field distance over the tumor and short high-intensity pulse sequence (mechanical index > 1.0) was used to destroy (flash) all MBs. Thereafter, low-intensity US imaging was performed again for 20 sec to capture tumor reperfusion of the MB contrast agent. After a 2 h delay to allow MB dissolution and clearance from the circulatory system, all animals that received targeted MBs during the first imaging session were reimaged using the control contrast agent and vice versa.

D. Image processing

Custom programs were developed using Matlab software (Mathworks Inc, Natick, MA) for processing post scan-converted US image data. For each dataset, an image visualization module displayed contrast-enhanced US images at a given time point in the transverse, sagittal, and coronal planes. After identifying the largest tumor cross-section in each orientation, a polygonal region-of-interest (ROI) was manually traced around the tumor boundary in each of the views. For simplicity, the final segmented tumor volume was derived numerically as the intersection set from projections of these three orthogonal planes and applied throughout the temporal dimension. A predefined image intensity threshold of 10% was applied to minimize background noise for all processed images. The mean voxel intensity from segmented pre-flash volumes was digitally subtracted from the post-flash volume data. This
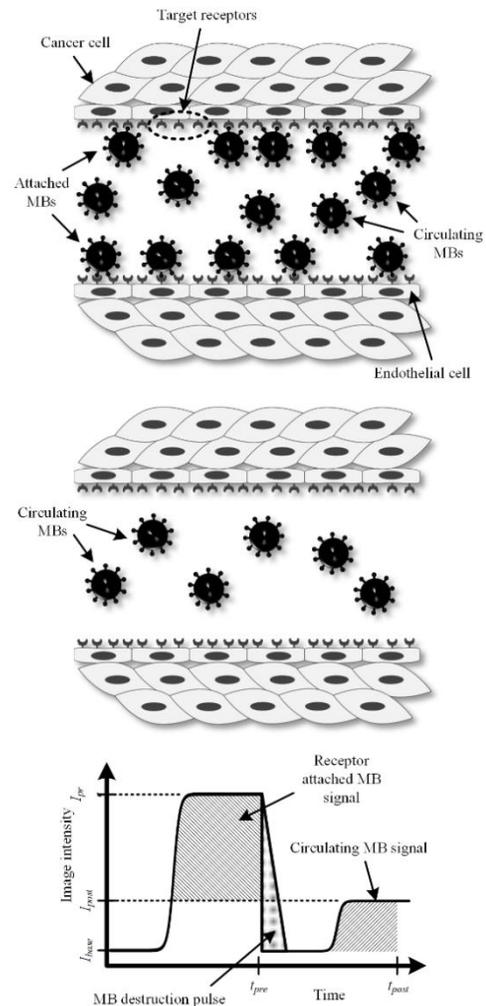
Fig. 1. Illustration of targeted US contrast agents attached to receptors over-expressed on tumor endothelial cells after intravenous administration and systemic circulation (top). A portion of injected MBs do not attach to the target receptors and freely circulate through tumor microvascularity. After destruction of all MBs in the tumor volume (both attached and freely circulating) using a high-intensity US pulse sequence, reperfusion with only freely circulating MBs occurs (middle). The difference in contrast-enhanced US image intensity before and after MB destruction is a surrogate measure of attached MBs to the target angiogenic biomarkers representing the molecular US signal (bottom).

image intensity difference determines the molecular US signal, Fig. 1. Additionally, fractional tumor enhancement (FTE) measures were computed as the percentage of voxels above the intensity threshold compared to the total number of voxels defining the segmented tumor space. Lastly, segmented tumor volumes were reconstructed and rendered for visualization purposes.

E. Immunohistology

All animals were euthanized after completion of the imaging study. Tumors from a random subset of nine animals were excised for immunohistologic analysis. Tumor tissue was formalin fixed and embedded in paraffin blocks. Serial sections of 5 μm thicknesses were cut from the blocks and transferred to glass slides (Super-Frost Plus, Fisher Scientific, Pittsburg, PA). Sections were stained with hematoxylin and eosin (H&E), and

CD31, VEGFR2, p-selectin, and $\alpha_V\beta_3$-integrin antibodies using techniques detailed previously [5]. H&E sections were examined by an experienced reader blinded to the experimental protocol to identify presence of cellular necrosis and to determine the percent of viable tumor tissue as a fraction of the entire tumor cross-section. Similarly, each CD31, VEGFR2, p-selectin, and $\alpha_V\beta_3$-integrin stained tissue section were reviewed to qualitatively identify the relatively dense stained regions which were delineated on the microscopy images and recorded as percent tissue stained of the entire tumor cross-section.

F. Statistical analysis

Data was summarized as mean ± standard error. The Wilcoxon signed-rank test was used to compare molecular US imaging results from animals injected with control and targeted MBs. A two-way ANOVA test evaluated differences in immunohistologic measurements. A relationship between US imaging and immunohistologic measurements was determined using a Spearman's correlation test. A p-value less than 0.05 was considered statistically significant.

III. RESULTS

From the original dataset of eighteen animals, data acquired from two animals was removed from further consideration due to a bad tail vein injection in one and incomplete MB contrast agent destruction in the other. Temporal sequences of whole tumor contrast-enhanced US images were collected in the same prostate cancer-bearing animals using both control and targeted microbubbles. MBs bound to select angiogenic receptors were evaluated for both contrast agent types to determine the utility of molecular US imaging of prostate cancer biomarkers. Representative volume reconstructions from whole tumor contrast-enhanced US imaging of MB presence in the same prostate tumor are illustrated in Fig. 2. For comparison, images are shown describing control and targeted MB contrast agent results both before and after agent destruction from the field-of-view (FOV). It is important to note that after a short 2 min delay following intravenous administration of the contrast media, targeted MBs produce a significant enhancement in ultrasound image intensity as compared to the same animal dosed with controls MBs ($p = 0.001$). These images reflect the detected ultrasound signal from both the freely circulating and biomarker bound MB contrast agents. The difference in image intensity before and after MB destruction was then used as surrogate
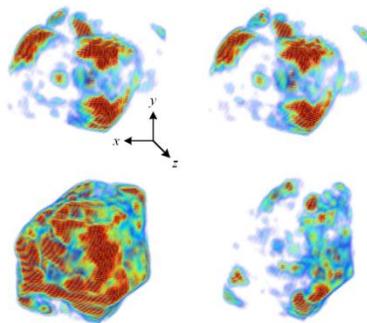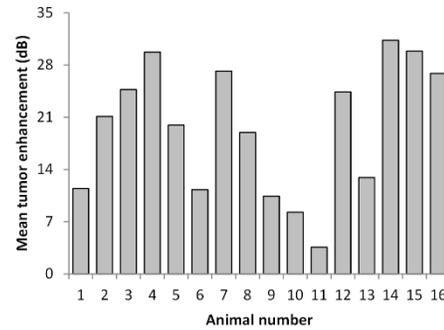
Fig. 3. Intrasubject molecular US signal gain measured as the relative differences in intratumoral image enhancement levels produced using targeted versus control MB contrast agents.

measure of the receptor (biomarker) bound MB contrast agents as this simple numerical technique functions as a pseudo filter for removing any undesirable signal from the freely circulating agents. The whole tumor molecular US signal measurements from the same animals, administered with either control or targeted MB contrast agents, were summarized. In general, molecular US signals were consistently higher when imaging the tumor angiogenesis with targeted MBs versus US imaging of control contrast agent (37.1 ± 3.9 and 5.8 ± 1.7, respectively; $p < 0.001$). Fig. 3 details the overall intra-animal molecular US signal gain (due to MB binding) computed as the relative difference in molecular US image enhancement using targeted and control MB contrast agents. Although noticeably variable from one animal to the next, a mean tumor enhancement of 19.5 ± 2.2 dB was found.

FTE measures were found to be $10.9 \pm 1.6\%$. While no correlation was found between the molecular US signal (using targeted MB contrast agent) and tumor volume measurements ($\rho = -0.05$, $p = 0.85$), there was a statistically significant inverse relationship between the molecular US signal and FTE ($\rho = -0.56$, $p = 0.02$), Fig. 4.

Immunohistologic results from processing excised prostate tumor samples were summarized. For the angiogenic receptors targeted during the molecular US imaging study, the average intratumoral density was found to be $63.9 \pm 4.9\%$, $59.1 \pm 6.4\%$, and $52.3 \pm 5.5\%$, for the VEGFR2, $\alpha_V\beta_3$-integrin, and p-selectin stained tissue samples, respectively ($p > 0.72$). Angiogenic receptors were found to be heterogeneous in spatial distribution.

Fig. 2. Rendered volumes from preclinical contrast-enhanced US imaging of prostate cancer (left) before and (right) after contrast agent destruction from the field-of-view. Imaging data was collected in the same tumor using both (top) control and (bottom) targeted MB contrast agents. Note MB accumulation using targeted agents compared to controls.
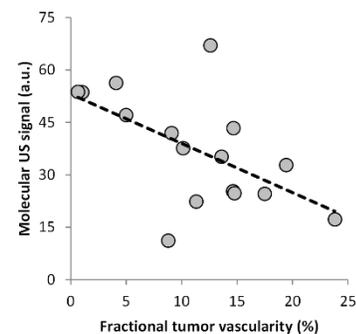
Fig. 4. Scatterplot describing the relationship between molecular US signal (using contrast agent targeted to angiogenic receptors) and fractional tumor enhancement (FTE) measurements in prostate cancer-bearing animals. A linear trendline is superimposed to assist visualization of the inverse relationship between imaging variables.

A correlation was not found between the molecular US signal and angiogenic immunohistochemistry measurements ($\rho < 0.27$, $p > 0.49$). No relationship was found between FTE values and VEGFR2 or $\alpha_V\beta_3$-integrin measurements ($\rho < 0.23$, $p > 0.55$). However, there was a significant correlation between tumor FTE and p-selection expression ($\rho = 0.80$, $p = 0.04$).

IV. DISCUSSION

This article described a volumetric molecular US imaging system using targeted MB contrast agents for detection of angiogenic imaging biomarkers associated with tumor growth. Custom image processing software was used to separate the backscattered US signal originating from intravascular MBs that were bound to the overexpressed biomarker targets from the freely circulating and unattached contrast agent. For the purpose of performance evaluation, molecular US imaging using targeted MBs was compared to US imaging results obtained using non-specific control MBs in the same animal. Consequently, it was found that molecular US imaging of the targeted MB contrast agent produced a considerable mean intratumoral enhancement of 19.5 ± 2.2 dB. Variability of signal enhancement between tumors is expected as vascularity differs, however the trend remains significant. This finding indicates whole tumor molecular US imaging is a sensitive modality for determining imaging biomarkers (FTE, molecular US image enhancement) associated with angiogenesis and cancer vascularity throughout the entire tumor burden.

FTE measures were found to be $10.9 \pm 1.6\%$ and consistent with the fact that tumor vascularity can be up to 10% of total tumor volume [3]. There was an inverse correlation between the molecular US signal and FTE ($\rho = -0.56$, $p = 0.02$), which suggests that as the spatial distribution of the molecular US signal increases, the average intensity of the same intratumoral reporter signal decreases. This finding is of particular interest because it could signify that when the neovascularity is inadequate to meet the metabolic demands of the tumor, there is a strong angiogenic response as detected using molecular US imaging. This strong angiogenic response is typically found in aggressive cancers and during the early (hypoxic) states of tumor growth. Therefore, molecular US imaging may improve US for the early detection of aggressive prostate cancers and guiding biopsy of suspicious lesions.

Analysis of immunohistologic results revealed a strong correlation between the molecular US imaging-based FTE measure and p-selection expression density ($\rho = 0.80$, $p = 0.04$) but not with VEGFR2 or $\alpha_V\beta_3$-integrin ($\rho < 0.23$, $p > 0.55$). Given FTE and the biomarker values are spatial density estimates, a stronger correlation can be expected although analysis of the later is inherently subjective. A limitation of the immunohistologic analysis was that it evaluated receptor expression throughout the entire tumor sample and did not restrict estimation to only endothelial cells which the targeted MB contrast agents attach to produce the molecular US signal. Future work should include a more detailed quantitative analysis of receptor expression from tumor specimens, which might reveal a stronger correlation between these receptor expression levels and results obtained using whole tumor molecular US imaging.

V. CONCLUSION

This study investigated the use of whole tumor molecular US imaging for the sensitive detection of tumor angiogenesis. With continued development of clinically translatable targeted MB contrast agents and advanced multi-dimensional imaging technology, molecular US imaging could emerge as a useful clinical resource. Over the next several years, there will be a growing demand for medical imaging equipment that eliminates unnecessary diagnostic procedures, reduces healthcare costs, and improves diagnostic accuracy. Molecular US imaging can clearly be positioned to address these demands.

REFERENCES

[1] N. Weidner, J. Folkman, F. Pozza, P. Bevilacqua, E. N. Allred, D. H. Moore, *et al.*, "Tumor angiogenesis: a new significant and independent prognostic indicator in early-stage breast carcinoma.," *J Natl Cancer Inst,* vol. 84, pp. 1875-87, Dec 1992.

[2] K. L. Weind, C. F. Maier, B. K. Rutt, and M. Moussa, "Invasive carcinomas and fibroadenomas of the breast: comparison of microvessel distributions--implications for imaging modalities.," *Radiology,* vol. 208, pp. 477-83, Aug 1998.

[3] R. K. Jain, "Barriers to drug delivery in solid tumors.," *Sci Am,* vol. 271, pp. 58-65, Jul 1994.

[4] J. A. Knowles, C. H. Heath, R. Saini, H. Umphrey, J. Warram, K. Hoyt, *et al.*, "Molecular targeting of ultrasonographic contrast agent for detection of head and neck squamous cell carcinoma," *Arch Otolaryngol Head Neck Surg,* vol. 138, pp. 662-8, Jul 2012.

[5] J. M. Warram, A. G. Sorace, R. Saini, H. R. Umphrey, K. R. Zinn, and K. Hoyt, "A triple-targeted ultrasound contrast agent provides improved localization to tumor vasculature.," *J Ultrasound Med,* vol. 30, pp. 921-31, Jul 2011.

[6] A. Sorace, R. Saini, M. Mahoney, and K. Hoyt, "Molecular ultrasound imaging using a targeted contrast agent for assessing early tumor response to antiangiogenic therapy.," *J Ultrasound Med,* vol. 31, pp. 1543-1550, 2012.

[7] R. Saini and K. Hoyt, "Recent developments in dynamic contrast-enhanced ultrasound imaging of tumor angiogenesis," *Imaging Med,* vol. 6, pp. 41-52, 2014.

[8] R. Saini, J. M. Warram, A. G. Sorace, H. Umphrey, K. R. Zinn, and K. Hoyt, "Model system using controlled receptor expression for evaluating targeted ultrasound contrast agents.," *Ultrasound Med Biol,* vol. 37, pp. 1306-13, Aug 2011.

[9] R. Saini, A. G. Sorace, J. M. Warram, M. J. Mahoney, K. R. Zinn, and K. Hoyt, "An animal model allowing controlled receptor expression for molecular ultrasound imaging," *Ultrasound Med Biol,* vol. 39, pp. 172-80, Jan 2013.

[10] J. E. Streeter, R. C. Gessner, J. Tsuruta, S. Feingold, and P. A. Dayton, "Assessment of molecular imaging of angiogenesis with three-dimensional ultrasonography," *Mol Imaging,* vol. 10, pp. 460-8, Dec 2011.

[11] K. Hoyt, A. Sorace, and R. Saini, "Quantitative mapping of tumor vascularity using volumetric contrast-enhanced ultrasound.," *Invest Radiol,* vol. 47, pp. 167-74, Mar 2012.

[12] M. Mahoney, A. Sorace, J. Warram, S. Samuel, and K. Hoyt, "Volumetric contrast-enhanced ultrasound imaging of renal perfusion," *J Ultrasound Med,* vol. 33, pp. 1427-1437, 2014.

[13] K. Hoyt, A. Sorace, and R. Saini, "Volumetric contrast-enhanced ultrasound imaging to assess early response to apoptosis-inducing anti-death receptor 5 antibody therapy in a breast cancer animal model," *J Ultrasound Med,* vol. 31, pp. 1759-66, Nov 2012.

ORIGINAL ARTICLE

A dual-reporter, diagnostic vector for prostate cancer detection and tumor imaging

JR Richter[1], M Mahoney[2], JM Warram[3], S Samuel[1] and KR Zinn[1]

Detection of prostate-specific antigen (PSA) as a screening strategy for prostate cancer is limited by the inability of the PSA test to differentiate between malignant cancer and benign hyperplasia. Here, we report the use of a cancer-specific promoter, inhibition of differentiation-1 (Id1), to drive a dual-reporter system (Ad5/3-Id1-SEAP-Id1-mCherry) designed for detection of prostate cancer using a blood-based reporter-secreted embryonic alkaline phosphatase (SEAP) and tumor visualization using a fluorescent reporter protein, mCherry. In human prostate tumors, Id1 levels are correlated with increased Gleason grade and disease progression. To evaluate the performance of the dual-reporter system, a prostate cell panel with varying aggressive phenotypes was tested. Following infection with the Ad5/3-Id1-SEAP-Id1-mCherry vector, expression of the SEAP and mCherry reporters was shown to increase with increasing levels of cellular Id1. No correlation was observed between Id1 and PSA. To evaluate in vivo performance, flank tumors were grown in athymic male mice using three prostate cancer cell lines. Following intra-tumoral injection of the vector, tumors formed by cells with high Id1 had the greatest reporter expression. Interestingly, tumors with the lowest levels of Id1 and reporter expression produced the greatest amounts of PSA. These data support the use of Ad5/3-Id1-SEAP-Id1-mCherry as a predictor of prostate cancer malignancy and as a strategy for tumor localization.

Gene Therapy advance online publication, 24 July 2014; doi:10.1038/gt.2014.68

INTRODUCTION

Since 1986, screening for prostate cancer has relied heavily on the detection of prostate-specific antigen (PSA) in the blood. The relative levels of PSA predict the abnormal presence of hyperplasia in the prostate. However, the PSA test cannot distinguish between lethal and non-lethal disease, owing to the low specificity of the test to differentiate aggressive cancer.[1–5] Considering these limitations, an improved method for prostate cancer screening is needed to accurately distinguish between aggressive and indolent cancers.

Inhibitor of differentiation (Id1) is a member of the inhibitor of differentiation family of transcription factors. They form inactive heterodimers with the basic helix–loop–helix family of transcription factors that control cellular processes, such as cell-fate determination, proliferation, cell-cycle regulation, angiogenesis, invasion and migration.[6,7] Id1 gene expression is cancer-specific and has been demonstrated to have increasing levels in human prostate tumors, which correlate with increasing Gleason grade and progression.[8,9] Several studies[10–14] have shown expression of Id1 to be an indicator of malignancy, with no expression found in cases of benign prostate hyperplasia and normal prostate tissue. The correlation between increased Id1 expression and cancer aggressiveness supports the use of the Id1 promoter for controlling diagnostic reporter function.

Recently, the diagnostic vector Ad5/3-Id1-SEAP-Id1-mCherry was constructed and shown to be highly specific and sensitive for breast cancer detection in both in vitro and in vivo models.[15,16] With this vector, dual-reporter expression of secreted embryonic alkaline phosphatase (SEAP) and the fluorescent protein mCherry is driven by the cancer-specific promoter Id1 and allows for both blood-based screening and localized visualization of cancer. Introduction of two Id1 promoters upstream of each reporter allows for equal and effective promoter control of SEAP and mCherry expression, which can be used in collaboration or independently. Furthermore, this diagnostic adenovirus (Ad) is designed to shuttle the reporter genes more effectively to cancer cells by replacement of the Ad5 fiber knob domain with that of the Ad3 fiber. This modification overcomes the limited availability of the native coxsackievirus and Ad receptor, which is commonly downregulated in cancer cells.[17]

SEAP is a truncated and secreted form of human embryonic alkaline phosphatase that is extremely stable and nonimmunogenic. Owing to its heat stability and resistance to the phosphatase inhibitor L-homoarginine, reporter SEAP levels can be measured independently from endogenous alkaline phosphatase activity with high sensitivity. The imaging reporter mCherry, has an excitation peak of 587 nm and emission peak of 610 nm, and is a mutated variant of the widely used mRFP1. The mCherry protein matures more quickly and completely than mRFP1, yielding a higher extinction coefficient and brightness, yet bleaches 10 times more slowly.[18] The longer wavelength of mCherry decreases the interference from tissue auto-fluorescence and allows for greater tissue penetration. mCherry can be detected by fluorescence imaging in the surgical setting using laparoscopic techniques, including robotic surgery (e.g., daVinchi), to improve surgical treatment of relevant prostate cancer. Importantly, as both the SEAP and mCherry reporters are under the control of Id1, reporter expression using the diagnostic vector Ad5/3-Id1-SEAP-Id1-mCherry is predicted to be an indicator of cancer prognosis.

[1]Department of Radiology, University of Alabama at Birmingham, Birmingham, AL, USA; [2]Department of Biomedical Engineering, University of Alabama at Birmingham, Birmingham, AL, USA and [3]Department of Surgery, University of Alabama at Birmingham, Birmingham, AL, USA. Correspondence: Dr KR Zinn, Departments of Medicine, Radiology, and Pathology, University of Alabama at Birmingham, Volker Hall G082, 1670 University Boulevard, Birmingham, AL 35294, USA.
E-mail: kurtzinn@uab.edu

In the present study, Ad5/3-Id1-SEAP-Id1-mCherry was evaluated as a diagnostic system for screening prostate cancer using normal cells and cancer cell lines of differing aggressive phenotypes. By correlating Id1 expression with SEAP levels and mCherry fluorescence, the effectiveness of Ad5/3-Id1-SEAP-Id1-mCherry in predicting cancer cell phenotype was compared with PSA results. In addition, the applicability of the diagnostic vector for in vivo cancer detection and localization was determined. The dual-reporter vector represents a novel method for non-invasively measuring cancer aggressiveness and visually monitoring prostate cancer, ultimately overcoming the limitations associated with PSA-based diagnoses.

RESULTS

Id1 expression, but not PSA level, is an indicator of prostate cancer cell aggressiveness

Six prostate cell lines were categorized based on their reported behaviors[19–24] and measured levels of PSA secretion (Table 1). Normal prostate cells (WPMY-1) secreted a baseline amount of 314.1 ± 8.1 pg ml^{-1} PSA. Two of the four cell lines with reportedly aggressive phenotypes (Du145 and PC3) had relatively lower PSA levels, ranging from 230 to 266 pg ml^{-1}, whereas the remaining aggressive cells lines (VCaP and MDA-PCA-2b) had significantly ($P < 0.001$) greater levels of PSA as compared with WPMY-1. The one non-aggressive cell type, LNCaP, also secreted significantly increased amounts of PSA in comparison with baseline levels. Id1 expression was elevated in all aggressive prostate cancer cell types compared with normal prostate cells and less-aggressive cells (Figure 1a). There was no statistical correlation between Id1 expression and PSA level ($P = 0.65$; Figure 1b).

SEAP and mCherry reporter expression correlate with Id1 levels and are indicators of prostate cell aggressiveness

A quantitative luciferase (luc) assay was performed to account for differences between cell lines in their susceptibility to infection with the tropism-modified Ad5/3 vector caused by possible differences in Ad3 receptor levels. The relative levels of infectivity of the Ad5/3-CMV-Luc vector for each cell type are shown in Figure 2a. These luciferase counts were subsequently used to normalize diagnostic reporter expression. SEAP and mCherry reporter expressions were therefore only a reflection of Id1 promoter activity. After infection with Ad5/3-Id1-SEAP-Id1-mCherry, the prostate cancer lines with aggressive phenotypes (VCaP, MDA-PCA-2b, PC3 and Du145) had increased levels of SEAP reporter compared with non-aggressive (LNCaP) and normal (WPMY-1) cells (Figure 2b). For PC3 and Du145, Ad3-normalized SEAP expression was significantly elevated at 4 and 6 days post infection compared with non-aggressive LNCaP cells at the corresponding time points. On the basis of the quantification of cellular Id1 presented in Figure 1a, the cell types were grouped based on low (< 0.25 a.u.), moderate (0.25–1.5 a.u.) or high (> 1.5 a.u.) Id1 levels in order to assess the relationship between SEAP reporter and Id1 promoter levels. Cells with moderate Id1 levels had increased SEAP reporter expression as compared with cells with low Id1. Cells with high Id1 levels had significantly increased SEAP reporter expression as compared with cells with moderate and low Id1 (Figure 2c). Likewise, representative fluorescent images of the mCherry reporter confirmed diagnostic vector efficiency (Figure 3). mCherry intensity corresponded to cellular Id1 levels, with the greatest fluorescence observed in the aggressive Du145 cells (49.1 ± 5.2 fluorescent counts), followed by VCaP cells (35.6 ± 7.5 fluorescent counts) and WPMY-1 cells (16.4 ± 3.5 fluorescent counts).

In vivo reporter expression correlates with prostate cancer malignancy despite PSA levels

To evaluate the potential of the vector to diagnose prostate cancer in vivo, flank tumors were formed using three different prostate cancer cell lines with low (LNCaP), moderate (PC3) and high (Du145) expression levels of Id1. At the time of vector injection, there were no significant differences in tumor size

Table 1. Description of cell lines used for analyses of Ad5/3-Id1-SEAP-Id1-mCherry diagnostic efficacy

Cell Line	Origin	Behavior	PSA (pg ml)[a]
WPMY-1	Normal stromal myofibroblast	Normal[16]	324.6 ± 21.5
Du145	Brain metastasis	Aggressive[17]	$230.1 \pm 8.3^{**}$
PC3	Bone metastasis	Aggressive[18]	$266.2 \pm 36.7^{*}$
VCaP	Vertebral metastasis	Aggressive[19]	$762.9 \pm 36.4^{**}$
MDA-PCA-2b	Bone metastasis	Aggressive[20]	$11{,}227 \pm 1274^{**}$
LNCaP	Node metastasis	Non-aggressive[21]	$13{,}042 \pm 315^{**}$

Abbreviation: PSA, prostate-specific antigen. [a]PSA values reported as mean $\pm$ s.e.m. ($n = 3$). $^{*}P < 0.05$ and $^{**}P < 0.001$ vs WPMY-1 level.
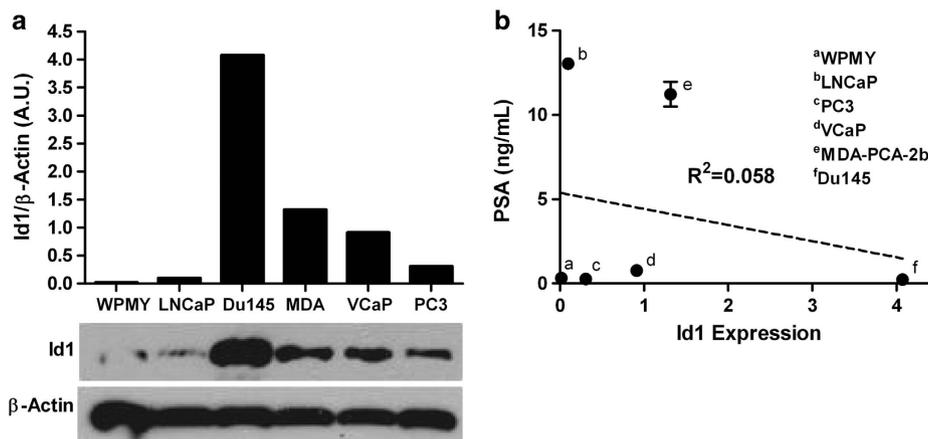
Figure 1. Id1 expression of the prostate cell panel and its lack of correlation with PSA. (a) Id1 expression was evaluated in cell lysates by western blot and quanitified with densitometry. Id1 intensity was normalized to the corresponding level of of β-actin. (b) Linear regression analysis was used to demonstrate no correlation between cellular Id1 levels and the PSA levels reported in Table 1. PSA data are shown as mean $\pm$ s.e.m. ($n = 3$).

Figure 2. SEAP reporter expression in the prostate cell panel and its relationship with cellular Id1. (**a**) Susceptibility for infection via the Ad3 fiber serotype was determined for each cell type using Ad5/3-CMV-Luc (multiplicity of infection = 1). Luciferase activity was used to normalize diagnostic reporter expression for differences in vector infectivity due to varying levels of Ad3 receptor expression. (**b**) SEAP reporter was measured in culture medium 2, 4 and 6 days post infection with Ad5/3-Id1-SEAP-Id1-mCherry (multiplicity of infection = 1) and normalized with luciferase activity. *$P < 0.01$ vs LNCap at corresponding time point. All data are reported as mean ± s.e.m. ($n = 4$). (**c**) Cells types were group based on low (< 0.25 a.u.), moderate (0.25–1.5 a.u.) or high (> 1.5 a.u.) Id1 levels and SEAP reporter expression averaged for each group. The low-Id1 group consisted of two cell types (WPMY-1 and LNCaP), the moderate-Id1 group consisted of three cells types (PC3, VCaP and MDA-PCA-2b) and the high-Id1 group consisted of one cell type (Du145). *$P < 0.01$ vs low and **$P < 0.001$ vs all groups.

between any of the groups (LNCaP: 207 ± 32 mm³; PC3: 203 ± 37 mm³; Du145: 171 ± 29 mm³). Elevated plasma levels of PSA were detected in mice bearing LNCaP tumors (1860 ± 144 pg ml⁻¹), whereas mice with PC3 and Du145 tumors did not have detectable amounts of PSA.

SEAP and mCherry reporter expression were monitored in all mice over a 14-day time period (Figures 4a and 5a). For SEAP

analyses, post-treatment levels were compared with baseline SEAP expression measured at day 0 prior to vector injection. Two days after intra-tumoral (IT) injection of Ad5/3-Id1-SEAP-Id1-mCherry, SEAP reporter expression was significantly elevated over baseline levels for the Du145 group, and mCherry reporter fluorescence permitted visual localization of these tumors. SEAP reporter expression was detectable in mice bearing PC3 tumors beginning 2 days after IT injection, and tumor fluorescence was detected at day 6. Post-treatment SEAP levels in mice with LNCaP tumors were slightly elevated above baseline levels beginning at day 6, and mCherry fluorescence was not observed in these tumors at any time point. The SEAP measured in plasma over the entire 14-day time course following vector injection was totaled to represent the effect of making multiple post-treatment diagnostic readings (Figure 4b). The combined effect of successive SEAP measurements revealed an elevated post-treatment SEAP level for each of the tumor types that was significantly greater than the baseline level. Furthermore, a proportional relationship between total amount of measured SEAP and tumor Id1 was observed, with tumors formed by Du145 cells leading to the highest plasma levels of the SEAP reporter and LNCaP tumors having the least. This trend was also observed with mCherry reporter expression, as Du145 tumors had the brightest tumor fluorescence at all time points followed by PC3 tumors and finally LNCaP tumors, which showed negligible mCherry expression (Figure 5). A representative image of the tumor fluorescence visualized at day 6 post vector injection is shown in Figure 5b.

DISCUSSION

Gene therapies have great potential for both treatment and diagnosis of cancer. In particular, the use of adenoviral vectors for molecular imaging of cancer offers opportunities to non-invasively gain information regarding tumor location as well as disease-specific information with regard to metabolism, receptor expression or tumor vascularity.[25] Much of the development and clinical application of viral-based vector strategies, however, has been limited by their associated immunogenicity, pathogenicity and natural tropism. The diagnostic Ad Ad5/3-Id1-SEAP-Id1-mCherry investigated in this work overcomes many of the challenges commonly associated with viral vectors, as it is replication defective and engineered to demonstrate enhanced cancer-specific infectivity. The hybrid Ad5/3 fiber of this vector ablates tropism of coxsackievirus and Ad receptor and overcomes its limited availability in cancer by introducing the Ad3 serotype fiber. Thus, the hybrid Ad5/3 fiber allows for improved and selective infectivity. In addition, as the dual-reporter system is under the control of the cancer-specific promoter Id1, reporter expression is designed to be cancer-specific and an indicator of prognosis.

The current work evaluated the ability of the dual-reporter vector, Ad5/3-Id1-SEAP-Id1-mCherry, to non-invasively detect and monitor prostate cancer using expression of a SEAP reporter for blood-based detection and mCherry reporter for fluorescence imaging. Using a panel of prostate cancer cells and normal prostate cells, it was demonstrated that, unlike PSA, cellular expression of both the SEAP and mCherry reporters was directly proportional to cellular levels of Id1. Given the direct relationship between the aggressive nature of cancer and Id1 expression, these findings support the use of Ad5/3-Id1-SEAP-Id1-mCherry for evaluating prostate cancer aggressiveness. *In vivo* studies confirmed the ability to measure blood-based levels of the SEAP reporter and to identify mCherry tumor fluorescence *in situ*. These results also confirmed that reporter expression correlated with Id1 levels and not the level of vector infectivity, as tumors formed by Du145 cells with high Id1 expression had the highest reporter levels and tumors formed by LNCaP cells with low Id1 expression had the lowest levels of reporter expression, despite a higher level of vector infectivity observed in LNCaP cells (Figure 2a).
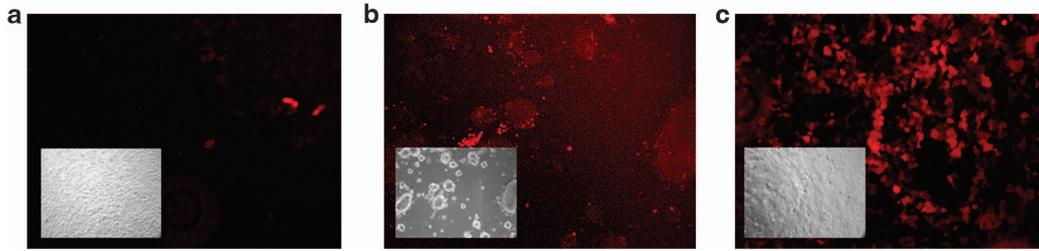
Figure 3. mCherry reporter fluorescence in normal prostate cells and cancerous cells with moderate and high levels of Id1. Representative fluorescence images of (**a**) normal prostate cells (WPMY-1) and cancerous cells with (**b**) moderate Id1 expression (VCaP) and (**c**) high Id1 expression (Du145). Inserts are corresponding bright-field images. All images were acquired using a ×10 objective.

Figure 4. *In vivo* SEAP reporter expression following IT injection of the diagnostic vector. (**a**) Plasma levels of the SEAP reporter were monitored over a 14-day period for tumors formed by prostate cancer cells with high (Du145), moderate (PC3) and low (LNCaP) levels of Id1. All data are reported as mean ± s.e.m. ($n = 5$). *$P < 0.001$ vs baseline and +$P < 0.01$ vs baseline (the order of stacked symbols correspond to order of data points). (**b**) SEAP amounts measured over the entire time course were totaled and compared with baseline levels measured before vector injection. *$P < 0.001$ vs baseline and +$P < 0.001$ vs LNCaP and PC3.

with as little as 7000 infected breast cancer cells.[15] The present work is proof of principle that this same diagnostic vector can be applied for detection of prostate cancer and that, similarly to the breast cancer model, reporter activity is driven by the Id1 promoter. Using IT injections of the Ad vector, this work demonstrates that tumor infectivity leads to production of the SEAP and mCherry reporters that are sufficiently distinguishable above background levels to aid in cancer detection and tumor visualization. Future studies will address the need for targeted delivery of the diagnostic vector to the tumor following systemic injection.

The *in vivo* time course analyses of SEAP and mCherry reporter expression following IT injection of the diagnostic vector revealed differences in the temporal translation of the dual-reporter system. Whereas SEAP levels appeared to peak at 3 days post injection, maximum mCherry tumor fluorescence was not observed until day 6 post treatment. These temporal differences in reporter expression could be potentially explained by the continual intracellular accumulation of the mCherry reporter accompanied by its slower degradation versus the immediate secretion of SEAP into the bloodstream, followed by its degradation and clearance. These data suggest that in cases of tumors with low to moderate levels of Id1, accumulation of mCherry is necessary to achieve a fluorescent signal that can be detected above background. This is evidenced by the fact that PC3 tumors with moderate Id1 levels were not visually detected before 6 days post injection, whereas Du145 tumors with high Id1 expression were visualized at the earliest time point. Given the unknown half-life of the blood-based SEAP reporter, the time course analyses do not delineate between SEAP accumulation and the production of newly made and expressed SEAP. However, it is clear from the LNCaP data presented in Figure 4 that, for potential clinical applications successive measurements over a series of several days may be required to assess reporter function and accurately define tumor behavior, especially for less-aggressive cancers.

The lower limit of detection for tumor visualization using mCherry fluorescence was not surpassed with LNCaP tumors. As reporter expression was dependent on cellular Id1 expression and LNCaP cells have relatively low levels of Id1, mCherry expression was not sufficient to produce a detectable fluorescent signal. The dependency of the diagnostic vector on adequate expression of Id1 represents a limitation of the current system for visually locating less-aggressive cancers. In future applications, non-aggressive prostate cancers could be diagnosed by non-elevated SEAP levels, however, visual localization of the cancer based on tumor fluorescence would be virtually impossible in the absence of sufficient Id1 activation. Likewise, tumor size (i.e., the number of cells available for transduction) is an important consideration for the prognostic application of this Ad vector, as reporter expression is proportional to cellular levels of Id1 within the tumor.

The present work introduces a novel strategy for detection and localization of prostate cancer that overcomes the current limitations of the PSA test to distinguish between aggressive cancer and indolent conditions, such as benign prostate

Furthermore, these data demonstrate that PSA was an inaccurate measure of cancer malignancy as the non-aggessive LNCaP tumors led to elevated plasma PSA, whereas the aggressive Du145 and PC3 cells had non-detectable levels of PSA. Together, these data suggest that the Ad5/3-Id1-SEAP-Id1-mCherry diagnostic vector could serve as a sensitive and non-invasive strategy for diagnosing prostate cancer that would overcome the current limitations associated with the PSA test by providing measures that are based on tumor cell aggressiveness.

Our previous work demonstrated the detection sensitivity of the Ad5/3-Id1-SEAP-Id1-mCherry diagnostic system, showing that the threshold value for detecting the SEAP reporter could be achieved

Figure 5. mCherry tumor fluorescence following IT injection of the diagnostic vector. (**a**) mCherry reporter expression for tumors formed by prostate cancer cells with high (Du145), moderate (PC3) and low (LNCaP) levels of Id1 was monitored and quantified over a 14-day time period. All data are reported as mean $\pm$ s.e.m. ($n = 5$). $^{+}P < 0.05$ vs PC3; $^{*}P < 0.01$ vs LNCaP; $^{\bullet}P < 0.05$ vs LNCaP. (**b**) Representative images of mCherry fluorescence at day 6 post IT injection of the diagnostic vector for LNCaP, PC3 and Du145 tumors.

hyperplasia. The correlation between reporter expression and cellular Id1 enables SEAP levels to be used as a predictive measure of prostate cancer aggressiveness, and mCherry fluorescence as an aid for tumor visualization. A major challenge of viral-based delivery systems for gene therapy applications is achieving targeted tumor delivery and sufficient infectivity. Future studies will develop strategies to target vector delivery and infectivity of both aggressive and non-aggressive prostate cancer. This strategy would assist clinicians in the detection and treatment of prostate cancer and ultimately reduce the mortality associated with this disease.

MATERIALS AND METHODS

Cell culture

The efficacy of the diagnostic vector was evaluated using six prostate cancer cell lines: WMPY-1, MDA-PCa-2b, VCaP, PC3, Du145 and LNCaP (American Type Culture Collection, Manassas, VA, USA). Two commonly used prostate cell lines (RWPE-1 and Ca-HPV-10) were excluded from the cell panel, due to immortalization vector HPV-18 interaction with endogenous Id1 protein.[26–28] LNCaP cells were maintained in RPMI-1640 with 10% fetal bovine serum (FBS) and 1% L-glutamine. Du145 cells were grown in Eagle's minimum essential medium with 10% FBS and 1% L-glutamine. VCap cells were maintained in Dulbecco's modified Eagle's medium containing 10% FBS and 1% L-glutamine. WMPY-1 cells were grown in Dulbecco's modified Eagle medium with 5% FBS and 1% L-glutamine. PC3 cells were grown in F12k basal medium with 10% FBS. MDA-PCa-2b cells were maintained in F12k basal medium containing 20% FBS, 25 ng ml^{-1} cholera toxin, 10 ngml^{-1} mouse epidermal growth factor, 5 nm phosphoethanolamine, 100 pgml^{-1} hydrocortisone, 45 nm selenious acid and 5 µg ml^{-1} bovine insulin. All cells were cultured at 37 °C and 5% CO$_2$. Cells were allowed to reach 75–90% confluency before passaging.

In vitro experiments

Cells (1.0×10^5 cells cm^{-2}) were plated in quadruplicate 24 h before infection with Ad5/3-Id1-SEAP-Id1-mCherry. Cells were infected at a multiplicity of infection ratio of one. Virus concentration (PFU ml^{-1}) was calculated based on the plaque-forming units using a standard agarose-overlay plaque assay. Media was collected at 2, 4 and 6 days post infection and SEAP levels measured using the Great EscAPe SEAP Fluorescence Detection kit (Clontech Laboratories, Mountain View, CA, USA). Media was also collected from uninfected cells to measure background fluorescence. In addition, PSA levels were quantified in the culture medium of each cell type by an enzyme-linked immunosorbent assay specific for human PSA (AbCam, Cambridge, MA, USA).

In order to qualify SEAP reporter expression as a singular function of Id1 promoter activity, a normalization assay was performed using an Ad5/3-CMV-Luc Ad to quantify vector infectivity. This Ad was generated using the same Ad5/3 adenoviral backbone used to construct the Ad5/3-Id1-SEAP-Id1-mCherry Ad. For all cell lines, 1.0×10^5 cells were infected with Ad5/3-CMV-Luc (multiplicity of infection = 1). Forty-eight hours post infection,

cells were imaged with an IVIS-100 CCD imaging system (Caliper Life Sciences, Mountain View, CA, USA). Matched region of interest analysis was performed using instrument software (Living Image 4.2, Xenogen, Hopkinton, MA, USA) to quantify total luciferase counts per well. Luciferase counts represented a relative level of Ad5/3 infectivity for each cell type and were subsequently used to normalize the SEAP measurements.

For data analysis, background fluorescence from uninfected cells was subtracted from the measured fluorescence of infected cells and SEAP levels were normalized to corresponding vector infectivity. To evaluate the relationship between SEAP reporter expression and cellular Id1, cells were grouped based on their level of Id1 expression as determined by western blot (low Id1 level: < 0.25 a.u.; moderate Id1 level: 0.25–1.5 a.u.; high Id1 level: > 1.5 a.u.). On the basis of these guidelines, the low-Id1 group consisted of WPMY-1 and LNCaP cells, the moderate-Id1 group consisted of PC3, VCaP and MDA-PCA-2b cells and the high-Id1 group consisted of Du145 cells. Day 4 SEAP reporter expression was averaged for the cell types in each group and compared.

Western blot

Protein lysates from all cell lines were collected with RIPA-modified buffer (Sigma-Aldrich, St Louis, MO, USA) with 1% SDS and phosphatase inhibitors (1 mM sodium orthovanadate, 25 mM b-glycerophosphate and 100 mM sodium fluoride) and protease inhibitors (10 mg ml^{-1} leupeptin, 10 mg ml^{-1} aprotinin and 1 mM phenylmethylsulfonyl fluoride). Protein lysates (15 µg, determined by the Lowry assay) were separated with 4–12% bis-Tris electrophoresis gel (Life Technology, Carlsbad, CA, USA), followed by transfer to polyvinylidene fluoride membranes (Millipore Immobilon, Billerica, MA, USA). Membranes were blocked with 5% bovine serum albumin and probed with rabbit monoclonal anti-mouse Id1, clone 195-14 (CalBioreagents, San Mateo, CA, USA), followed by horseradish peroxidase-conjugated goat anti-rabbit Ig (SouthernBiotech, Birmingham, AL, USA). All membranes were washed three times with tris-buffered saline and tween 20 buffer for 20 min per wash. Id1 protein was visualized using chemiluminescent substrate (SuperSignal West Pico Chemiluminescent Substrate, ThermoScientific, Rockford, IL, USA). Densitometry was performed using ImageJ software (version 1.47t, National Institutes of Health, Bethesda, MD, USA), and Id1 levels were normalized to the respective β-actin controls.

In vivo analyses

Animal studies were performed in accordance with the National Institutes of Health recommendations and the approval of the Institutional Animal Care and Use Committee at the University of Alabama at Birmingham. Athymic male nude mice were obtained from Frederick Cancer Research (Hartford, CT, USA). Flank tumors were grown over a 6–8-week time period following implantation of 4×10^6 prostate cancer cells (LNCaP, PC3 or Du145). For implantation of PC3 and Du145 cells, the cells were harvested, resuspended in cold phosphate-buffered saline and injected subcutaneously into the left flank. The gelatin sponge Vetspon (Novartis Animal Health, Greensboro, NC, USA) was used to facilitate LNCaP tumor development. For inoculation of LNCaP cells with Vetspon, the material was cut to 0.5 cm^3 and 4×10^6 cells in 0.15 ml cold phosphate-buffered

saline were seeded into the Vetspon by gently pipetting until the cells were completely absorbed. A small incision was created on the left flank and the cell-soaked Vetspon placed under the skin. The wound was closed with two prolene sutures. Mature tumors were injected intra-tumorally with 1×10^9 PFU of the diagnostic vector Ad5/3-Id1-SEAP-Id1-mCherry. To measure SEAP reporter expression, blood was collected retro-orbitally into heparinized capillary tubes and plasma levels of SEAP measured using the Great EscAPe Detection kit (Clontech Laboratories). SEAP levels and mCherry tumor fluorescence were monitored on days 2, 3, 6, 10 and 14 post injection.

Fluorescence imaging

Representative *in vitro* fluorescent images were acquired on day 2 post infection with Ad5/3-Id1-SEAP-Id1-mCherry. Cell images (×100) were rendered using an mCherry 587 nm excitation/600-nm-long pass filter on an inverted microscope with a halogen light source and Nuance multi-spectral camera (CRi, Woburn, WA, USA). A liquid-crystal tunable wavelength filter in the camera was set for collection of emission images from 600 to 720 nm in 5-nm increments. Composite images (unmixed composites) were generated for each image cube by unmixing the spectral signature of the mCherry reporter from those of background auto-fluorescence. For *in vivo* images, mice were anesthetized with isoflurane and tumors were imaged with a Leica stereomicrosope (Model MZ-FLIII, Vashaw Scientific, Norcross, GA, USA). Filter, camera and image processing from the *in vitro* imaging methods were used in coordination with the stereomicroscope. Quantitative region of interest analysis for mCherry fluorescence with background subtraction was performed with ImageJ software and total counts from size-matched regions of interest were recorded.

Statistical analyses

Results are reported as the mean plus or minus s.e.m. Data were analyzed for statistical significance using the Student's *t*-test or analysis of variance with Bonferroni's multiple comparison test where appropriate using Prism (version 6.0, GraphPad Software, La Jolla, CA, USA). For statistical analyses of PSA data, values for the normal prostate cells (WPMY-1) were used as a baseline PSA level and comparisons with baseline were made using the Student's *t*-test. Linear regression analysis was used to evaluate the correlation between PSA levels and cellular Id1. For *in vivo* quantification of the mCherry reporter, background fluorescence was subtracted from the fluorescence intensity of the infected tumors. Student's *t*-tests were used to make pairwise comparisons of *in vivo* mCherry tumor fluorescence and SEAP expression.

CONFLICT OF INTEREST

The authors declare no conflict of interest.

REFERENCES

1 Grubb 3rd RL, Pinsky PF, Greenlee RT, Izmirlian G, Miller AB, Hickey TP *et al.* Prostate cancer screening in the Prostate, Lung, Colorectal and Ovarian cancer screening trial: update on findings from the initial four rounds of screening in a randomized trial. *BJU Int* 2008; **102**: 1524–1530.

2 Schroder FH, Hugosson J, Roobol MJ, Tammela TL, Ciatto S, Nelen V *et al.* Screening and prostate-cancer mortality in a randomized European study. *N Engl J Med* 2009; **360**: 1320–1328.

3 Abrahamsson PA, Artibani W, Chapple CR, Wirth M. European Association of Urology position statement on screening for prostate cancer. *Eur Urol* 2009; **56**: 270–271.

4 Smith RA, Cokkinides V, Brooks D, Saslow D, Brawley OW. Cancer screening in the United States, 2010: a review of current American Cancer Society guidelines and issues in cancer screening. *CA Cancer J Clin* 2010; **60**: 99–119.

5 Lin K, Lipsitz R, Miller T, Janakiraman S, Force USPST. Benefits and harms of prostate-specific antigen screening for prostate cancer: an evidence update for the U.S. Preventive Services Task Force. *Ann Intern Med* 2008; **149**: 192–199.

6 Sun XH, Copeland NG, Jenkins NA, Baltimore D. Id proteins Id1 and Id2 selectively inhibit DNA binding by one class of helix-loop-helix proteins. *Mol Cell Biol* 1991; **11**: 5603–5611.

7 Pesce S, Benezra R. The loop region of the helix-loop-helix protein Id1 is critical for its dominant negative activity. *Mol Cell Biol* 1993; **13**: 7874–7880.

8 Yu X, Xu X, Han B, Zhou R. Inhibitor of DNA binding-1 overexpression in prostate cancer: relevance to tumor differentiation. *Pathol Oncol Res* 2009; **15**: 91–96.

9 Coppe JP, Itahana Y, Moore DH, Bennington JL, Desprez PY. Id-1 and Id-2 proteins as molecular markers for human prostate cancer progression. *Clin Cancer Res* 2004; **10**: 2044–2051.

10 Ouyang XS, Wang X, Lee DT, Tsao SW, Wong YC. Over expression of ID-1 in prostate cancer. *J Urol* 2002; **167**: 2598–2602.

11 Ouyang XS, Wang X, Lee DT, Tsao SW, Wong YC. Up-regulation of TRPM-2, MMP-7 and ID-1 during sex hormone-induced prostate carcinogenesis in the Noble rat. *Carcinogenesis* 2001; **22**: 965–973.

12 Darby S, Cross SS, Brown NJ, Hamdy FC, Robson CN. BMP-6 over-expression in prostate cancer is associated with increased Id-1 protein and a more invasive phenotype. *J Pathol* 2008; **214**: 394–404.

13 Ling MT, Wang X, Lee DT, Tam PC, Tsao SW, Wong YC. Id-1 expression induces androgen-independent prostate cancer cell growth through activation of epidermal growth factor receptor (EGF-R). *Carcinogenesis* 2004; **25**: 517–525.

14 Zhang X, Ling MT, Wang X, Wong YC. Inactivation of Id-1 in prostate cancer cells: a potential therapeutic target in inducing chemosensitization to taxol through activation of JNK pathway. *Int J Cancer* 2006; **118**: 2072–2081.

15 Warram JM, Borovjagin AV, Zinn KR. A genetic strategy for combined screening and localized imaging of breast cancer. *Mol Imaging Biol* 2011; **13**: 452–461.

16 Warram JM, Sorace AG, Saini R, Borovjagin AV, Hoyt K, Zinn KR. Systemic delivery of a breast cancer-detecting adenovirus using targeted microbubbles. *Cancer Gene Ther* 2012; **19**: 545–552.

17 Kanerva A, Mikheeva GV, Krasnykh V, Coolidge CJ, Lam JT, Mahasreshti PJ *et al.* Targeting adenovirus to the serotype 3 receptor increases gene transfer efficiency to ovarian cancer cells. *Clin Cancer Res* 2002; **8**: 275–280.

18 Shaner NC, Campbell RE, Steinbach PA, Giepmans BN, Palmer AE, Tsien RY. Improved monomeric red, orange and yellow fluorescent proteins derived from Discosoma sp. red fluorescent protein. *Nat Biotechnol* 2004; **22**: 1567–1572.

19 Bello D, Webber MM, Kleinman HK, Wartinger DD, Rhim JS. Androgen responsive adult human prostatic epithelial cell lines immortalized by human papilloma-virus 18. *Carcinogenesis* 1997; **18**: 1215–1223.

20 Papsidero LD, Kuriyama M, Wang MC, Horoszewicz J, Leong SS, Valenzuela L *et al.* Prostate antigen: a marker for human prostate epithelial cells. *J Natl Cancer Inst* 1981; **66**: 37–42.

21 Kaighn ME, Narayan KS, Ohnuki Y, Lechner JF, Jones LW. Establishment and characterization of a human prostatic carcinoma cell line (PC-3). *Invest Urol* 1979; **17**: 16–23.

22 Korenchuk S, Lehr JE, MClean L, Lee YG, Whitney S, Vessella R *et al.* VCaP, a cell-based model system of human prostate cancer. *In vivo* 2001; **15**: 163–168.

23 Navone NM, Olive M, Ozen M, Davis R, Troncoso P, Tu SM *et al.* Establishment of two human prostate cancer cell lines derived from a single bone metastasis. *Clin Cancer Res* 1997; **3**: 2493–2500.

24 Gibas Z, Becher R, Kawinski E, Horoszewicz J, Sandberg AA. A high-resolution study of chromosome changes in a human prostatic carcinoma cell line (LNCaP). *Cancer Genet Cytogenet* 1984; **11**: 399–404.

25 Zinn KR, Chaudhuri TR. Imaging adenovirus-mediated gene transfer. In: Curiel DT, Douglas JT (eds). *Adenoviral Vectors for Gene Therapy*. Elsevier Science: San Diego, CA, 2002, pp 655–677.

26 Alani RM, Hasskarl J, Grace M, Hernandez MC, Israel MA, Munger K. Immortali-zation of primary human keratinocytes by the helix-loop-helix protein, Id-1. *Proc Natl Acad Sci USA* 1999; **96**: 9637–9641.

27 Yasmeen A, Bismar TA, Kandouz M, Foulkes WD, Desprez PY, Al Moustafa AE. E6/E7 of HPV type 16 promotes cell invasion and metastasis of human breast cancer cells. *Cell Cycle* 2007; **6**: 2038–2042.

28 Akil N, Yasmeen A, Kassab A, Ghabreau L, Darnel AD, Al Moustafa AE. High-risk human papillomavirus infections in breast cancer in Syrian women and their association with Id-1 expression: a tissue microarray study. *Br J Cancer* 2008; **99**: 404–407.